Atmos. Chem. Phys. Discuss., 12, 3295–3356, 2012
www.atmos-chem-phys-discuss.net/12/3295/2012/
doi:10.5194/acpd-12-3295-2012

Atmospheric Chemistry and Physics Discussions

Multi-generation gas-phase oxidation, equilibrium partitioning, and the formation and evolution of secondary organic aerosol

C. D. Cappa[1] **and K. R. Wilson**[2]

[1]Department of Civil and Environmental Engineering, University of California, Davis, CA 95616, USA
[2]Chemical Sciences Division, Lawrence Berkeley National Laboratory, Berkeley, CA 94720, USA

Received: 11 January 2012 – Accepted: 19 January 2012 – Published: 31 January 2012

Correspondence to: C. D. Cappa (cdcappa@ucdavis.edu)

Published by Copernicus Publications on behalf of the European Geosciences Union.

Abstract

A new statistical model of secondary organic aerosol (SOA) formation is developed that explicitly takes into account multi-generational oxidation as well as fragmentation of gas-phase compounds. The model framework requires three tunable parameters to describe the kinetic evolution of SOA mass, the average oxygen-to-carbon atomic ratio and the mean particle volatility as oxidation proceeds. These parameters describe (1) the relationship between oxygen content and volatility, (2) the probability of fragmentation and (3) the amount of oxygen added per reaction. The time-evolution and absolute value of the SOA mass depends sensitively on all three tunable parameters. Of the tunable parameters, the mean O:C is most sensitive to the oxygen/volatility relationship, exhibiting only a weak dependence on the other two. The mean particle O:C produced from a given compound is primarily controlled by the number of carbon atoms comprising the SOA precursor. It is found that gas-phase compounds with larger than 11 carbon atoms are unlikely to form SOA with O:C values >0.4, which suggests that so-called "intermediate-volatility" organic compounds (IVOCs) and "semi-volatile" organic compounds (SVOCs) are not major contributors to the ambient SOA burden when high O:C ratios are observed, especially at short atmospheric times. The model is tested against laboratory measurements of SOA formation from the photooxidation of α-pinene and *n*-pentadecane and performs well (after tuning). This model may provide a generalized framework for the interpretation of laboratory SOA formation experiments in which explicit consideration of multiple-generations of products is required, which is true for all photo-oxidation experiments.

1 Introduction

Atmospheric aerosol particles play a key role in the Earth's climate system by absorbing and scattering solar radiation and influencing properties of clouds (IPCC, 2007). The influence of aerosols on climate depends on their composition, yet much remains

ACPD
12, 3295–3356, 2012

unknown with respect to formation, chemical evolution and removal pathways, especially when considering organic aerosols (OA) (Jacobson et al., 2000; Seinfeld and Pankow, 2003; Kanakidou et al., 2005). A primary challenge in developing comprehensive quantitative understanding of organic aerosols derives from their high chemical complexity, which results from there being a myriad of sources. Individual particles can be composed of numerous compounds, including organics, inorganics and soot; OA has both primary (i.e., direct emission, POA) and secondary (i.e., gas-to-particle conversion, SOA) sources and may be comprised of hundreds of different compounds (Kanakidou et al., 2005).

In the context of traditional equilibrium partitioning theory, the extent to which an organic compound partitions to the particle phase depends on the temperature-dependent volatility (Pankow, 1994) which varies over orders of magnitude for compounds in aerosols (e.g., Cappa et al., 2007, 2008). Quantitative understanding of the partitioning of organics between the gas and particle phase has been thought to be essential for accurately predicting the spatial and temporal distribution of OA in the atmosphere. However, typical models of OA formation in the atmosphere have tended to predict significantly less OA than is commonly observed (de Gouw et al., 2005; Heald et al., 2005; Johnson et al., 2006; Volkamer et al., 2006; Matsui et al., 2009). Recent updates to models of OA to include e.g., semi-volatile primary OA (Robinson et al., 2007) or new estimates of aerosol yields for aromatics (Ng et al., 2007) have led to somewhat better model/measurement agreement in terms of the total OA mass (Dzepina et al., 2009). However, the physical properties of the model OA are inconsistent with observations of OA volatility, with the model aerosol often being too volatile (Dzepina et al., 2009, 2011) or with too low an oxygen-to-carbon (O:C) ratio (Hodzic et al., 2010; Dzepina et al., 2011). When models do appear to give reasonable apparent volatilities they tend to use unrealistic input parameters (e.g., enthalpies of vaporization; Jathar et al., 2011). Models that appear to give reasonable values for O:C typically assume very large increases in mass upon reaction of a volatile organic compound (VOC) with OH, e.g., 40 % per reaction, all of which is assumed to be oxygen (Grieshop et al., 2009;

ACPD
12, 3295–3356, 2012

Hodzic et al., 2010; Dzepina et al., 2011). This suggests that, although there may be better agreement with observations of OA mass using updated models, the agreement may be fortuitous. This is problematic since model aerosol that is too volatile will respond to perturbations (such as dilution or temperature fluctuations) in unrealistic ways, which could lead to incorrect estimates of air quality and climate effects of particles.

In this study, the development of a new model of gas-phase hydrocarbon oxidation coupled to secondary OA formation via gas-particle partitioning is described. This model is used to explore the limits of gas-phase oxidation for producing the internal properties of OA, specifically volatility and the O:C ratio. The model results suggest that there is an inherent limitation to the maximum particle-phase O:C and minimum volatility that can be achieved via gas-phase processing alone. These results provide insights into the sources and pathways associated with ambient OA formation. In Sect. 2, a description of the model is given. In Sect. 3, the model is run to explore the influence of specific tunable parameters on the model results and to develop generalized understanding of SOA formation. In Sect. 4, the model is used to demonstrate the utility of the model framework by explicitly simulating laboratory measurements of SOA formation from the photooxidation of α-pinene and of *n*-pentadecane.

2 Model description

The statistical oxidation model (SOM) developed here treats the oxidation of a hydrocarbon as a statistical process and frames the oxidation chemistry as a trajectory through a multi-generational space defined by the number of carbon and oxygen atoms comprising the SOA precursor and all possible product molecules. Our model is, in some ways, a hybrid of the conceptual carbon-oxidation state model of Kroll et al. (2011), the 1 and 2-D volatility basis set (VBS) model of Donahue and co-workers (Donahue et al., 2006, 2011; Robinson et al., 2007; Jimenez et al., 2009) and the carbon number-polarity grid of Pankow and Barsanti (Pankow and Barsanti, 2009), all placed into an explicit kinetic framework. It is, in essence, a simplified and condensed

ACPD
12, 3295–3356, 2012

version of the explicit gas-phase photochemistry models that have been developed (e.g., Aumont et al., 2005) and shares some similarities with kinetic implementations of the VBS (e.g., Robinson et al., 2007; Lane et al., 2008) or the carbon number-polarity grid (Barsanti et al., 2011). It is, nonetheless, unique in the way that the oxidation process is represented and tracked through multiple generations of oxidation.

Within the SOM, functionalization reactions produce molecules with the same number of carbon atoms (N_C) as the parent compound but a larger number of oxygenated functional groups. Fragmentation reactions lead to C-C bond scission and the formation of two smaller molecules, where the total number of carbon and oxygen atoms are conserved. The distribution of compounds between the gas and particle phase is treated through equilibrium partitioning theory (Pankow, 1994). In the model all compounds are allowed to react with OH radicals, with the exception of compounds with a single carbon atom (e.g., CO, CO_2, etc.), which represent the end points of oxidation and are assumed to be inconsequential for SOA formation. In other words, every compound represents a molecule that is both formed and consumed by OH, with the exception of the initial SOA precursor. (Although all products could therefore be considered "SOA precursors", we restrict this term to mean the initial, unreacted hydrocarbon.)

Neither hydrogen atoms nor functional groups are explicitly considered; instead average molecular properties are specified for the "molecules" that populate a matrix of all possible N_C and N_O combinations (up to a limit of $N_O/N_C = 2$). Each cell in the matrix effectively represents an average of some number of e.g., ketones, alcohols, peroxides. The relationship between "structure" (i.e., the number of carbon and oxygen atoms) and a given property (e.g., volatility or reactivity towards OH) are tunable parameters in the model. The specific tunable parameters in our model are as follows:

1. The average number of oxygen atoms added per reaction.
2. The decrease in vapor pressure (volatility) per oxygen added.
3. The probability of a given product fragmenting.

ACPD
12, 3295–3356, 2012

These parameters, which govern the trajectory that the oxidation takes through the carbon/oxygen space, can be envisioned as unique to a given reaction (e.g., dodecane + OH). Together these parameters will determine the absolute value of and temporal variation in gas and particle phase oxidation products, ultimately determining the aerosol yield, the average O:C ratio and the average volatility of the OA. In a sense, these tunable parameters are related to the specification of a volatility basis-set (Donahue et al., 2006, 2011) or "two-product model" (Odum et al., 1996), but now explicitly formulated to account for the kinetics of oxidation and the formation of multiple-generations of gas and particle-phase reaction products.

A unique aspect of the SOM is that the structure of individual "molecules" are determined (i.e., N_C and N_O), and the properties of these molecules are specified based on their "structure" to determine the evolution of the gas/particle system throughout a reaction. This can be contrasted to kinetic implementations of the VBS, which relate property to structure (if structure is specified at all), or to kinetic implementations of the N_C-polarity grid, which requires as input product structures and associated yields (Barsanti et al., 2011).

Traditionally, the oxidation of hydrocarbons has been discussed in the context of "generations" of oxidation (Ng et al., 2006). However, because oxidation products are themselves reactive towards OH, products with relatively large numbers of oxygen atoms always have some probability of being formed, even early on in the reaction. This is simply a consequence of statistical oxidation in a well-mixed system. For example, for the case where all molecules react with OH with the same rate coefficient (k_{OH}), the distribution of oxidation products at any point in the reaction can be described as a simple Poisson Distribution, as recently shown by Wilson et al. (2012). Note that "generation" is equal to the number of times that a molecule has reacted, starting from the initial SOA precursor. Further, because more than 1 oxygen-containing functional group can be added per reaction, the number of oxygens per molecule is not necessarily equal to the number of "generations" of oxidation.

ACPD
12, 3295–3356, 2012

For a single SOA precursor, it is useful to follow the evolution of the system with respect to loss of the SOA precursor, which can be quantified by the number of "oxidation lifetimes", (lifetimes = $\tau_{OH} = [OH]/k_{OH}$, where [OH] is the concentration of OH radicals, assumed to be constant). The distribution of product molecules formed from any SOA precuror is continuously evolving throughout a reaction in both the gas and particle phases. In the SOM, these time-dependent distributions are explicitly computed as the reaction proceeds. The exact form and kinetic evolution of these distributions depend on how the model is parameterized as described above. For example, the distribution of gas and particle phase molecules formed in a generic photooxidation reaction is shown in Fig. 1. For illustrative purposes, fragmentation is neglected and it is assumed that only 1 oxygen functional group is added per reaction. Thus the number of oxygens (N_O) is equal to the generation number, n. Before reaction, there is only gas-phase material with the number of carbon atoms (N_C) equal to the SOA precursor and $N_O = 0$. Upon reaction, a small amount of 1st, 2nd, ..., n-th generation products are produced almost instantaneously, even after little of the SOA precursor hydrocarbon has been consumed (i.e., at $\tau_{OH} \ll 1$). Since higher-n generations have lower volatility (i.e., more oxygen for the same N_C), the particle phase distribution at this point is dominated by these compounds, which reside at the tail-end of the product distribution, even though they make up a negligible amount of the total mass. As the reaction continues, the total abundance of these later-generation products increases, producing a broader distribution of product generations that evolve towards larger average n with increasing oxidation. As the total abundance of any given n-th generation product increases, the amount that partitions to the particle phase will also increase, thus accelerating the total amount of OA that is formed (Pankow, 1994).

In the absence of SOA formation, the distribution of the gas-phase products would evolve approximately as a Poisson distribution (Smith et al., 2009; Wilson et al., 2012). However, with SOA formation the relative abundances of the products in either phase evolves in a more complex manner since molecules are generated through gas-phase reactions and are then partitioned between the gas and particle phases according to

ACPD
12, 3295–3356, 2012

their abundance and volatility. Also, the absolute abundance of any given product molecule or generation does not increase indefinitely. Over time, just as the absolute abundance of the SOA precursor decreases from reaction with OH, the absolute abundance of any given gas-phase *n*-th generation product also decreases as these molecules react with OH to form higher generation products.

Figure 1 reveals how the distribution of specific compounds (generations) continuously evolves during oxidation due to reactions of both the SOA precursor and product molecules, which indicates that the yield of a given compound is not static. This result is not surprising, since all products are assumed to react with OH, but this aspect is often neglected in the interpretation of traditional aerosol yield experiments where it is implicitly assumed (although not always stated) that product distributions are static. Figure 1 illustrates the statistical nature of oxidation as well as the importance of considering the formation and evolution of product distributions in both the gas and particle phases during photooxidation.

The model developed herein takes into account the time-evolution of the product distributions, in contrast to traditional 2-product or more recent static VBS parameterizations of aerosol yields. Although this would seemingly suggest greater complexity of the SOM, the number of tunable parameters is limited (to two constants and 1 array), and thus similar to these other formulations (4 parameters for a 2-product model; Odum et al., 1996, or, typically, 4 parameters for the VBS model; Donahue et al., 2006). The details of how molecules move through the carbon-oxygen matrix for a specific photooxidation reaction will depend explicitly on how these tunable parameters are specified. A key feature of the SOM is that it is possible to do this in a physically realistic manner and to test the validity of any parameterization against smog chamber measurements of SOA yield and composition. Below we outline how various parameters are assigned to the individual molecules within the distribution.

ACPD
12, 3295–3356, 2012

2.1 Kinetic parameterization of compound reactivity

All molecules in the carbon/oxygen matrix are assumed to be reactive with OH. Each "molecule" or product generation in the carbon/oxygen matrix has a unique rate coefficient that depends on the length of the carbon backbone and the number of oxygen atoms. The rate coefficients are computed using a modified version of typical structure-activity relationships (Kwok and Atkinson, 1995), where it is assumed:

$$k_{OH} = 2\, k_{prim}\, f_{CH_2} + (N_C - 2)\, k_{sec}\, f_{CH_2}^2 \text{ if } N_O = 0 \quad (1a)$$

$$k_{OH} = 2\, k_{prim} + (N_C - 2 - N_O)\, k_{sec} + 0.5\, N_O\, k_{tert}\, f_{OH} \text{ if } N_O > 0 \text{ and } N_O < N_C - 2 \quad (2b)$$

$$k_{OH} = k_{prim} + 0.5\, N_O\, k_{tert}\, f_{OH} \text{ if } N_O = N_C - 1 \quad (3c)$$

$$k_{OH} = 0.5\, N_O\, k_{tert}\, f_{OH} \text{ if } N_O = N_C \quad (4d)$$

$$k_{OH} = 0.5\, (2\, N_C - N_O)\, k_{tert}\, f_{OH} \text{ if } N_O > N_C \quad (5e)$$

where $k_{prim} = 1.43 \times 10^{-13}$ cm^3 molecules^{-1} s^{-1}, $k_{sec} = 8.38 \times 10^{-13}$ cm^3 molecules^{-1} s^{-1}, $k_{tert} = 1.82 \times 10^{-12}$ cm^3 molecules^{-1} s^{-1}, $f_{CH_2} = 1.29$ and $f_{OH} = 3.6$ (Kwok and Atkinson, 1995). The "prim", "sec" and "tert" refer to primary, secondary and tertiary carbon atoms, respectively, while "OH" and "CH_2" refer to the oxygen containing and non-oxygen containing bonds, respectively. The need for this modified structure-activity relationship arises because the model does not explicitly keep track of the types of functional groups formed, and thus cannot use parameters unique to the addition of a ketone or alcohol, for example. The above equation is based on the reactivity of alkanes and approximates the addition of equal numbers of ketone and alcohol functional groups (this is where the 0.5 comes from in Eqs. 1b–e). For a $N_C = 12$ alkane-like hydrocarbon the calculated $k_{OH} = 1.43 \times 10^{-11}$ molecule cm^{-3}, which can be compared with the measured $k_{OH} = 1.32 \times 10^{-11}$ for dodecane (Atkinson, 2003). In principle, the modified k_{OH}-structure relationship can be altered to account for any specific starting

ACPD
12, 3295–3356, 2012

compound where, for example, the presence of double bonds may make the reactivity of the SOA precursors much larger than that of the products. Alternatively, reactions of alkenes with O_3 can be represented by setting the rate coefficients of the products to zero (assuming only 1 double bond is present).

2.2 Gas-particle partitioning and compound volatility

At each time step in the model, the system is assumed to achieve gas-particle equilibrium, which can be described through partitioning theory (Pankow, 1994). The extent of partitioning for a given compound is governed by the saturation concentration, C^*:

$$C_i^* = \frac{\mathrm{MW}_i \, p_{\mathrm{sat},i} \, \zeta_i}{R \, T} \tag{5}$$

where MW_i is the molecular weight ($\mathrm{g\,mol^{-1}}$), R is the ideal gas constant ($8.314\,\mathrm{J\,mol^{-1}\,K^{-1}}$), T is the temperature (K), ζ_i is the activity coefficient in the OA phase and $p_{\mathrm{sat},i}$ is the (sub-cooled liquid) saturation vapor pressure (Pa) of compound i (which may also represent a class of compounds). We assume ζ_i is unity, and thus C^* can best be thought of as an effective saturation concentration. In the general model formulation, hydrogen atoms are accounted for in the MW_i by using saturated hydrocarbons when $N_O = 0$ and assuming the number of hydrogen atoms decreases by 1 for each oxygen added; because of the much larger mass of carbon and oxygen atoms, this assumption has a negligible influence on the model results. In addition to C^*, the specific distribution of compounds between the particle and gas-phases depends on both the gas and particle phase abundance of that compound ($C_{i,\mathrm{tot}} = C_{i,\mathrm{gas}} + C_{i,\mathrm{aer}}$, gas + aerosol) and the total organic aerosol concentration (C_{OA}) according to (Liang and Pankow, 1996):

$$C_{\mathrm{OA}} = \sum_i C_{i,\mathrm{tot}} \left(1 + \frac{C_i^*}{C_{\mathrm{OA}}}\right)^{-1}. \tag{6}$$

ACPD
12, 3295–3356, 2012

It is well known that p_{sat} (and thus C^*) depends primarily on the length of the carbon backbone and the number and type of functional groups, and secondarily on specific molecular structure (Pankow and Asher, 2008). The addition of a ketone to a hydrocarbon backbone leads to a decrease in vapor pressure by a factor of ~10–20, an alcohol by a factor of ~160, and with the addition of a carboxylic acid group simply the product of these two. Previous work shows that the addition of all of these functional group types to SOA-forming hydrocarbons is possible, with some indication that, on average, equal numbers of ketones and alcohols are added (Heald et al., 2010), or that alcohol and carboxylic acid moieties are more prevalent than ketones (Ng et al., 2011; Russell et al., 2011), although under low-NO_x conditions hydroperoxides may also contribute.

In the SOM, only the number of carbon and oxygen atoms is considered rather than specific functional groups. This is because the framework of our model is a carbon/oxygen grid, so we consider the change in vapor pressure on a per oxygen basis rather than on a per functional group basis. Since the addition of a single oxygen-containing moiety decreases the vapor pressure by orders of magnitude, we will use the logarithmic change in vapor pressure, termed ΔlVP, throughout. For example, it follows that $\Delta lVP_1 \sim 1$ corresponds to the addition of one oxygen atom as a ketone group (a factor of 10 decrease), while $\Delta lVP \sim 2.23$ corresponds to an alcohol group (a factor of 160 decrease) (Pankow and Asher, 2008).

The oxygen/volatility relationship (i.e., ΔlVP) is a tunable parameter in the model. However, it is constrained to the range of possible ΔlVP values that fall within the range bounded by ketones ($\Delta lVP = 1$) and alcohols ($\Delta lVP = 2.23$). Note that hydroperoxides would have a $\Delta lVP \sim 1.24$ while nitrate groups would have a $\Delta lVP \sim 0.74$, both on a per-oxygen basis (Pankow and Asher, 2008). The base volatility of the carbon backbone is calculated as $\log_{10} C^* = -0.0337 MW_{HC} + 11.56$ (determined from data in Lide and Kehiaian, 1994), where MW_{HC} is the molecular weight of the SOA precursor carbon backbone, including hydrogen atoms.

ACPD
12, 3295–3356, 2012

2.3 Functionalization

Functionalization reactions are considered through the addition of oxygen upon reaction with OH in the presence of O_2. The number of oxygen atoms added per reaction is a tunable parameter within the model. It is assumed that the OH reaction leads to a distribution of functionalized products where 1, 2, 3 or 4 oxygens can be added as a result of the single OH attack. The probability of adding any given number of oxygen atoms is specified, with the total probability of oxygen addition summing to unity (i.e., reactions always lead to oxygen addition). For example, if it is assumed that a single OH reaction leads to a distribution of products where 50 % have added 1 oxygen, 50 % 2 oxygens and no contributions from 3 or 4 oxygens, the functionalization probability array would have the form $P_{\text{func}} = [1, 2, 3, 4] = [0.5, 0.5, 0.0, 0.0]$. Note that it is straight-forward to translate the distribution of generations shown in Fig. 1 to number of oxygens if it is assumed that only *n*-oxygens are added per reaction (and no fragmentation), but if a distribution of oxygens is added per reaction, then generation number and oxygen content cannot be shown in such a simple manner.

Again, the type of functional group added (e.g., ketone vs. alcohol) is not explicitly tracked. However, once the oxygen/volatility relationship is specified, one can in principle infer the average number of hydrogen atoms in any grid cell in the carbon/oxygen matrix. Recently, there has been interest in understanding how OA evolves in the space defined by the H:C and O:C ratio, i.e., a "van Krevelen" plot (e.g., Heald et al., 2010); any given point in this space can be characterized by the mean oxidation state, defined as $OS_C = 2\,O{:}C - H{:}C$ (Kroll et al., 2011). OS_C is implicitly a part of the SOM because, by specifying a specific value for ΔIVP the evolution of the hydrogen content of the system is effectively constrained. The addition of an alcohol functional group increases O:C but leaves H:C unchanged, whereas the addition of a ketone decreases H:C and increases O:C. If the ΔIVP is viewed simply as a linear combination of ketone and alcohol group addition, then the evolution of the hydrogen content (and thus of OS_C) can be determined. This, of course, ignores contributions of hydroperoxides or

ACPD
12, 3295–3356, 2012

other functional groups but can provide a first order constraint on the mean OA OS_C. For example, if ΔIVP = 1.6, this corresponds approximately to equal addition of ketones and alcohols. So, for the addition of 1 oxygen to an alkane SOA precursor, the functionalized product will have lost, on average, 1 hydrogen atom. By specifying ΔIVP, the slope in a van Krevelen plot is essentially being specified a priori; if ΔIVP = 1 then the van Krevelen slope is −2, whereas if ΔIVP = 2.2 the van Krevelen slope is 0.

2.4 Fragmentation

There is a probability that reaction with OH will lead to C-C bond scission, fragmenting the SOA precursor into two, smaller molecules. Because fragmentation is generally considered to be more likely when OH attack occurs near an already existing oxygenated functional group, the probability of fragmentation of a given molecule upon reaction is parameterized as:

$$P_{\text{frag}} \text{ (per reaction)} = c_{\text{frag}} N_{\text{O}} \tag{7}$$

where c_{frag} is a tunable parameter. The functional form of this fragmentation operator is found to be preferable to that proposed in Jimenez et al. (2009) ($P_{\text{frag}} = (N_{\text{O}}/N_{\text{C}})^{1/6}$) since this operator predicts very large fragmentation probabilities for small molecules (which have large O:C ratios for the addition of even a few oxygen atoms) and results in run-away fragmentation, making it very difficult to form SOA from small N_{C} compounds. The linear dependence on N_{O} (Eq. 4) prevents small molecules from excessively fragmenting upon the addition of the first oxygen. However, other functional forms for P_{frag} are possible and have been tested, such as a more general variation on the Jimenez et al. (2009) relationship:

$$P_{\text{frag}} \text{ (per reaction)} = \left(\frac{N_{\text{O}}}{N_{\text{C}}}\right)^{m_{\text{frag}}} \tag{8}$$

ACPD
12, 3295–3356, 2012

where m_{frag} is a constant (that is larger than 1/6). As will be shown in Sect. 4, both functional forms provide good agreement with observations. Determination of the preferred functional form for P_{frag} is the subject of future work.

Upon fragmentation, the distribution of product molecules amongst all possible choices is computed in one of two ways. (1) A random probability for the location of the C-C bond scission and thus the resulting size of the scission product. The corresponding species is then deduced from what atoms remain so as to achieve mass balance. (2) Fragmentation leads to production of only C_1 species, (i.e., CO_2 HCHO, CO, or CH_4), along with the appropriate co-product. The first method rapidly distributes mass amongst the entire carbon/oxygen matrix, whereas the second method more slowly leads to the production of fragments with N_C much less than the SOA precursor. As with the addition of distributions of oxygens per reaction, fragmentation further complicates the relationship between generation number and oxygen content, and requires specific consideration of the distribution of molecules in a 3-D space defined by N_C, N_O and abundance, with properties of every molecule (i.e., N_C/N_O pair) explicitly specified according to the relationships defined in the previous sections.

3 Results and discussion

3.1 Oxidation trajectories through the carbon/oxygen space

3.1.1 No fragmentation

A model run is first used to consider the case where no fragmentation ($c_{frag} = 0$) occurs. In this case, reactions of the gas-phase SOA precursor with OH will lead to the production of products with the same carbon number (N_C), as illustrated in Fig. 1. Starting from a single compound (e.g., dodecane), the rate at which the overall system (gas + particle) adds oxygen is controlled by the functionalization array, P_{func}. However,

ACPD
12, 3295–3356, 2012

the rate at which the aerosol becomes oxygenated will additionally be determined by the instantaneous aerosol mass loading, the specific compound volatilities and the assumed ΔIVP. As oxidation proceeds, increasing amounts of lower volatility (higher N_O) products in the distribution will be produced.

Products with lower volatility partition more strongly to the particle-phase than comparably higher volatility compounds. Aerosol composition depends on these volatility differences and the absolute abundance of each compound. The evolution of the particle composition depends on the interplay of these two factors, along with the variation in the total C_{OA}. Without fragmentation, the ability to add oxygen to the particle phase is limited by the decreasing volatility of the products upon oxygen addition. There is an upper limit to the addition of oxygen that is governed by partitioning theory since once a compound becomes of sufficiently low volatility (i.e., >99 % partitioned to the particle phase) the rate of gas-phase oxidation becomes negligible and further oxygen addition becomes slow. Ultimately, this limit is governed almost entirely by the combination of the SOA gas-phase precursor N_C and the assumed ΔIVP per reaction.

For a fixed value of ΔIVP, the variation in O:C with N_C can be calculated and has a fixed relationship that is controlled almost entirely by partitioning. Synthesis of field observations of O:C and H:C for ambient aerosol suggests that, on average, ketone (or aldehyde) and alcohol groups make up SOA in approximately equal abundances (Heald et al., 2010) or that alcohols are added with slightly greater frequency (Ng et al., 2011). (Note that the addition of e.g., hydroperoxides will alter the O:C/H:C relationship somewhat.) The former corresponds to a mean ΔIVP of ∼1.6. In broad terms, SOA precursors can be classified as volatile organic compounds (VOC, $C^* > 10^6\ \mu g\,m^{-3}$), intermediate volatility organic compounds (IVOC, $10^6\ \mu g\,m^{-3} > C^* > 10^3\ \mu g\,m^{-3}$) or as semi-volatile organic compounds (SVOC, $C^* < 10^3\ \mu g\,m^{-3}$) (Jathar et al., 2011). Using these designations, saturated hydrocarbons with $N_C < 12$ are VOCs, $12 \le N_C < 18$ are IVOCs and $N_C \ge 18$ are SVOCs (Fig. 2a). Previously unaccounted for contributions of IVOCs and SVOCs have been invoked to explain some of the "missing mass" in air quality or chemical transport models, with some models now suggesting that

ACPD
12, 3295–3356, 2012

contributions from these species account for more than half the OA burden in many regions, including global averages (Jathar et al., 2011).

The O:C vs. N_C relationship has been calculated assuming ΔIVP = 1.0, 1.6 or 2.2 and no fragmentation. Results are reported after 10 h of reaction assuming that (1) $\tau_{OH} = 1$ for the SOA precursor at 10 h, (2) $C_{OA} = 10\,\mu g\,m^{-3}$ at 10 h and (3) only 1 oxygen is added per reaction. The initial SOA gas-phase precursor concentration (termed $[HC]_0$) was adjusted for every ΔIVP value to achieve $C_{OA} = 10\,\mu g\,m^{-3}$ at 10 h. The $\tau_{OH} = 1$ assumption constrains [OH] to be around 2×10^6 molecules cm^{-3}, a typical daytime value. There is a direct relationship between N_C and the calculated mean O:C, with smaller N_C values producing aerosol with larger O:C (Fig. 2b). The variation in O:C with N_C for a given ΔIVP follows a power law relationship. The calculated O:C has some dependence on ΔIVP and is somewhat larger for smaller ΔIVP, although the overall range is relatively small, especially for larger carbon number SOA precursors. This is an expected result since an SOA precursor must react more times (add more oxygen) in order to achieve sufficiently low volatility to partition to the aerosol when ΔIVP is small.

There is a direct relationship between the calculated aerosol yield and both N_C and ΔIVP. (Aerosol yield is defined as $C_{OA}/[HC]_0$.) Larger N_C produce larger yields, as has previously been observed for reactions of alkanes under high-NO_x conditions (Jordan et al., 2008). (The smaller yields calculated here result primarily from the much lower C_{OA} in the calculations vs. the experiments.) Larger ΔIVP also results in higher yields for a given N_C (Fig. 2c). Since C_{OA} for all simulations was the same, this variation in yield is driven entirely by the need for larger $[HC]_0$ values at smaller ΔIVP; as ΔIVP decreases a greater amount of initial (gas-phase) mass is needed to produce a fixed amount of aerosol after one lifetime.

The explicit time evolution of the mean particle O:C is considered to understand how this intensive property is expected to vary throughout a typical laboratory photooxidation experiment. Results are shown for $N_C = 12$ assuming ΔIVP = 1.6 and 1 oxygen added per reaction and using $[HC]_0 = 195\,\mu g\,m^{-3}$ at $[OH] = 1.94 \times 10^6$ molecules cm^{-3}

ACPD
12, 3295–3356, 2012

(which gives 10 $\mu g\,m^{-3}$ over 10 h = 1 lifetime). Initially, the O:C is near zero and then increases rapidly, before plateauing and slowly decreasing with time (Fig. 3a). However, if only the period where $C_{OA} > 0.01\ \mu g\,m^{-3}$ is considered, which is below the detection of most modern instrumentation, the O:C is seen to continuously, albeit very slowly decrease as aerosol forms (Fig. 3b). This behavior is due to a competition between the production rate of lower-volatility species with high O:C and the increase in C_{OA}, which as it increases enhances the partitioning of somewhat higher volatility species with lower O:C to the particle phase. However, it is not only the increasing C_{OA}, but also the increasing concentrations of the individual product molecules that drives up the particle-phase abundance. Overall the variation in O:C with C_{OA} over the range pertinent to the atmosphere (i.e., measurable) is relatively small, with O:C over the range $0.1\ \mu g\,m^{-3} < C_{OA} < 10\ \mu g\,m^{-3}$ decreasing from 0.33 to 0.27. The magnitude of this decrease does depend somewhat on N_C; larger decreases are generally found for smaller N_C compounds (not shown). There is some dependence of the O:C results on the assumed $[HC]_0$. For example, if smaller $[HC]_0$ values are specified to give smaller C_{OA} after 10 h of reaction than above, the O:C is generally slightly larger than that calculated at an equivalent C_{OA} during the $C_{OA} = 10\ \mu g\,m^{-3}$ simulations (up to O:C = 0.36 at $0.1\ \mu g\,m^{-3}$; Fig. 3b).

Figure 2b indicates that only those compounds with ~11 or fewer carbon atoms produce OA with O:C > 0.4 after 1 lifetime of oxidation, which corresponds approximately to an atmospheric timescale of approximately 1–2 days at $\sim 2 \times 10^6$ molecules cm^{-3}. To obtain an O:C > 0.8, which has been observed for the most oxidized organic aerosol factor in ambient measurements (Ng et al., 2011), requires the SOA precursor to have less than 6 carbon atoms. The model results suggest that gas-phase processing of IVOC's and SVOC's (with $N_C \leq 12$) will primarily lead to the formation of SOA with relatively low O:C values (<~0.4) at these levels of oxidation, neglecting any fragmentation reactions, which will be considered below.

ACPD
12, 3295–3356, 2012

3.1.2 Fragmentation included

In principle, C-C bond scission reactions should lead to OA with a higher O:C than without fragmentation. This is because smaller molecules require more oxygen in order to partition to the particle phase. In the model, it is possible to explicitly consider to what extent this might occur. It must be emphasized that fragmentation will not only influence O:C, but will also impact the calculated aerosol yield as well as the kinetics of aerosol growth.

The role of fragmentation is considered using the $N_C = 12$ SOA precursor as a test case. The probability of fragmentation is varied by adjusting the parameter c_{frag} in Eq. (4) and by assuming either random fragmentation (case 1) or "small fragments" (case 2). (The general results are unchanged if the P_{frag} expression in Eq. 5 is instead used.) Two situations will be considered, one (case A) where the $[HC]_0$ is fixed and one (case B) where $[HC]_0$ is adjusted for each value of c_{frag} to keep C_{OA} (10 h) = 10 μg m^{-3}. For case A, $[HC]_0$ is selected to give C_{OA} (10 h, $\tau_{OH} = 1$) = 10 μg m^{-3} when $c_{frag} = 0$. In all cases it is assumed that ΔIVP = 1.6.

The primary finding is that, for all of the possible combinations of the above cases, the calculated O:C varies only over a very small range. Interestingly, the inclusion of fragmentation actually often leads to a *decrease* in the O:C. Consider cases 1B and 2B. In going from $c_{frag} = 0$ to $c_{frag} = 0.4$, the O:C (at 10 h) decreases from 0.27 to 0.22 or 0.25, respectively. For both cases 1A and 2A, the O:C increases slightly from 0.27 to 0.29 as c_{frag} increases from 0 to 0.2. However, for cases 1A and 2A, the amount of aerosol produced at 10 h drops precipitously, to 5.2 and 1.5 μg m^{-3} (case 2A) or 6.1 and 2.8 μg m^{-3} (case 2B), as c_{frag} increases to 0.1 or 0.2, respectively. Thus, fragmentation has a much larger influence on the calculated aerosol yield than it does on the O:C and fragmentation in the gas-phase is found to be a very inefficient way to increase the O:C of SOA.

ACPD
12, 3295–3356, 2012

There is a variety of molecular evidence to suggest that fragmentation occurs during photooxidation of SOA precursors (such as the observation of formaldehyde, formic acid or other small molecules during a photooxidation experiment; Lee et al., 2006). Thus, it is likely that if fragmentation is not included aerosol yields will be over-predicted (for a given $[HC]_0$), especially for small N_C compounds. A model that does not include fragmentation would likely find it necessary to use a lower value of ΔIVP in order to reduce the yield. However, this would likely lead to a slight over-prediction of the aerosol O:C and, more importantly, would also influence the time-evolution of the OA formation. Similarly, a model that assumed the fragmentation probability to be too large (such as if $P_{frag} = (O:C)^{1/6}$) will have difficultly forming OA for small N_C compounds.

Since intuition might suggest that the O:C of OA should increase when fragmentation is included, it is important to consider in some detail why this is not the case. First, although fragmentation does lead to the production of species that have a higher O:C before partitioning to the particle phase (i.e., species with $N_C <$ SOA precursor), these species ultimately contribute very little to the total OA mass. For the specific cases considered above, approximately 80 % of the OA mass is comprised of compounds with N_C equal to the SOA precursor compound. Much of the material with N_C equal to the SOA precursor condenses efficiently to the particle phase before fragmentation, which by itself limits the gas-phase production rate of smaller N_C compounds. Additionally, the fragments themselves have a greater probability of fragmenting prior to condensation because they persist longer in the gas-phase and undergo additional reactions to obtain a sufficiently high oxygen content to facilitate efficient condensation. In other words, the more times that a molecule reacts, the more chances it has to fragment (i.e., the total fragmentation probability for a given molecule is the product of the $1 - P_{frag}$ terms for prior reactions). Finally, because we assume that the probability of fragmentation scales with oxygen content, for even the N_C = SOA precursor, fragmentation will serve to depress somewhat the formation of the highest O:C species. In Fig. 4 the probability distribution of having *n*-oxygens per molecule in the particle-phase is shown for the no-fragmentation and the small fragments case (case 2B). Overall, fragmentation

ACPD
12, 3295–3356, 2012

moves the oxygen distribution towards molecules with fewer oxygen atoms, at least on the $\tau_{OH} = 1$ timescale considered here (the behavior at larger τ_{OH} is considered in Sect. 3.1.5).

If the same calculations are performed for other N_C compounds (from 5–20 carbon atoms), it is found that, in general, fragmentation leads to a small reduction in O:C for $N_C > 11$ and a slight increase for $N_C < 9$ (see Fig. 2b, calculated assuming $c_{frag} = 0.2$ and C_{OA} (10 h) = 10 µg m^{-3}). Again, fragmentation does not lead to a significant change in the mean particle O:C. However, fragmentation does strongly influence the calculated aerosol yield, with the influence of fragmentation becoming greater as N_C decreases (Fig. 5). As already discussed, fragmentation suppresses OA formation and thus a greater amount of initial hydrocarbon is necessary to produce the same C_{OA} at a given OH exposure. This serves to decrease the aerosol yield. The effect is much more pronounced for small compounds that must undergo many more gas-phase reactions than larger ones before sufficient oxygen is added to facilitate efficient condensation. Fragmentation will have a more pronounced influence on yields if smaller values of ΔIVP are assumed because, again, molecules must go through more reactions to add sufficient oxygen.

Thus, the overall influence of fragmentation is largest for small compounds and when ΔIVP is assumed to be small. Additionally, if the fragmentation probability (i.e., c_{frag}) is assumed to be larger, the ratio between yields without and with fragmentation grows. If the P_{frag} becomes large enough, OA formation by small compounds can be completely suppressed. If we assume, for example, that $P_{frag} = (O:C)^{1/6}$ (Jimenez et al., 2009) it is nearly impossible to form SOA from compounds with $N_C < 10$ without assuming large ΔIVP values. Future work will be focused on constraining the fragmentation operator based on laboratory smog chamber aerosol growth experiments, although preliminary analysis indicates that c_{frag} is ~0.25 (or that $m_{frag} \sim 0.4$; see Sect. 4).

To relate the output of the SOM to other model formulations, such as the VBS, the distributions of individual compounds can be binned by mass into logarithmically spaced C^* bins, and the evolution of this distribution throughout a reaction can be

ACPD
12, 3295–3356, 2012

calculated. An example is shown in Fig. 6 for the $N_C = 12$ simulation from above (Case 2b), although now the simulation has been run for many more lifetimes of oxidation (up to $\tau_{OH} = 5$ is shown). The distribution of products comprising both the total and the particle-phase only are continuously evolving, as expected given the continued reactivity of the products. The evolution of the total mass provides a visual example of the statistical nature of the oxidation process in the SOM (similar to that in Fig. 1), while the particle-phase shows the combined effects of volatility, the abundance of compounds in a given log C^* bin and the total C_{OA}. This provides a clear indication that the product yields are not static as a reaction proceeds, and has implications for the interpretation of laboratory aerosol yield curves when such interpretations are formulated in terms of static yields, as with the 2-product model (Odum et al., 1996) or VBS (Donahue et al., 2006).

3.1.3 Oxygen addition

In the previous sections, it was assumed that each reaction with OH led to the addition of only 1 oxygen atom. In this case, for a molecule to obtain e.g., 5 oxygens it would undergo at least 5 reactions. It is possible for some reactions to add more than 1 oxygen, most notably for the oxidation of aromatic compounds or of compounds containing double bonds, but also potentially for saturated compounds. In the SOM, up to 4 oxygen atoms can be added per reaction, where we assume, given the molecular complexity of oxidation mechanisms, that some distribution of oxygen atoms are added per reaction (e.g., 50 % add 1 oxygen and 50 % add 2 oxygens). Below, the influence of the assumed number of oxygens per reaction on the O:C and aerosol yield is explored.

Consider a SOA precursor compound that adds 1, 2, 3 or 4 oxygens per reaction. The more oxygens that are assumed to be added per reaction, the faster that the system will form "low" volatility compounds that can condense efficiently to the particle phase. Further, if fragmentation is included, because compounds that add more oxygen atoms per reaction ultimately go through fewer reactions prior to condensation, the influence of fragmentation is suppressed. This is true even though P_{frag} for an

ACPD
12, 3295–3356, 2012

individual species is assumed to be proportional to N_O, since it is the net fragmentation probability that most matters to the system (which is determined by the combination of the number of reactions and the specific P_{frag} values). As a specific example, again a $N_C = 12$ SOA precursor is used. The variation in C_{OA}, aerosol yield and O:C have been calculated for addition of 1, 2, 3 or 4 oxygens per reaction. The $[HC]_0$ were selected to produce $C_{OA} = 10\,\mu g\,m^{-3}$ after 3 oxidation lifetimes (30 h at 2×10^6 molecules cm^{-3}), assuming $\Delta IVP = 1.6$ and no fragmentation. Additional calculations were performed assuming that $P_{func} = [0.25, 0.25, 0.25, 0.25]$, or that $\Delta IVP = 1.0$ or 2.2 for 1 oxygen per reaction for comparison.

The assumed number of oxygens per reaction has a strong influence on the temporal evolution of the aerosol mass and the shape of yield and growth curves (Fig. 7). For example, there is a long time-lag before significant OA forms for the 1-oxygen case, whereas for the 4-oxygen case OA is formed nearly instantaneously. This difference should not be surprising, since the addition of more oxygen atoms per reaction leads to more rapid production of sufficiently low volatility material, and thus OA will form at a faster rate. However, it does suggest an important result, namely that the shape of a growth curve and the temporal evolution of OA formation can together be used to deduce the approximate number of oxygens added per reaction for a given system. Consider the low-NO_x oxidation of toluene, as an example (Ng et al., 2007). For this system, the growth curve (i.e., C_{OA} vs. $\Delta[HC]$) is nearly linear, suggesting that 3 or 4 oxygens are added per reaction, which is consistent with the low-NO_x oxidation mechanism (Ng et al., 2007).

Traditionally, growth curves are presented as C_{OA} vs. $\Delta[HC]$, the amount of SOA precursor reacted. To facilitate comparison with results from the SOM as well as between different experiments, growth curves should instead be presented with the x-axis as a fraction of the total initial hydrocarbon reacted (f_{HC}), rather than as an absolute change in the hydrocarbon concentration. By using f_{HC}, one can more easily identify the point at which all of the hydrocarbon has reacted. Previous work has argued that an increase in C_{OA} when f_{HC} approaches 1 is an indication of contributions of "second-generation"

ACPD
12, 3295–3356, 2012

products (Ng et al., 2006). However, as is clear from the SOM results, at any point in the reaction there is a statistical distribution of multiple generations of products in photo-oxidation experiments. Thus the continued SOA growth as $f_{HC} \rightarrow 1$ is due to production not only of second-generation products, but formation and continued simultaneous evolution of many generations of products. This is in contrast to O_3 + alkene oxidation experiments, where it really is second-generation products being formed (for systems that have two double bonds).

There is a relatively weak dependence of O:C on the assumed oxygens per reaction (Fig. 7d), although the specific dependence is non-intuitive. Consider that, for the $N_C = 12$ case here, the 3-oxygens per reaction case gives the highest O:C. This is because the $N_C = 12$, $N_O = 3$ compound has a volatility of $C^* = 10.7\,\mu g\,m^{-3}$. At $C_{OA} = 10\,\mu g\,m^{-3}$, a significant amount of material remains in the gas-phase available to undergo further reactions that add 3 additional oxygens. For the 4-oxygens per reaction case, the very low volatility of the first-generation products makes subsequent gas-phase reactions and oxygen addition very slow. As with the 4-oxygens per reaction case, for 1 or 2 oxygens per reaction the oxygen addition is slow once the precursor gas has added 4 oxygens. However, the molecular complexity of oxidation reactions suggests that a distribution of oxygens per reaction will likely be added, and thus, although illustrative, the cases considered above may not be general. To address this, calculations have been performed where it is assumed that 1, 2, 3 and 4 oxygens are added per reaction with equal probability. In this case, the O:C evolves approximately as an average of the individual cases (Fig. 7d).

The number of oxygen atoms added per reaction is not the only factor that controls the shape of yield or growth curves. The specific value of ΔIVP also influences the temporal evolution of the system by altering the rate at which sufficiently low volatility material is produced. The influence of ΔIVP can be assessed by recalling that the likely range over which ΔIVP varies is from 1 to 2.2 (a Δ of 1.2), which can then be compared to the influence of adding an additional oxygen. For a fixed ΔIVP, every additional oxygen will decrease the volatility by ΔIVP, which will usually be greater

ACPD
12, 3295–3356, 2012

than the difference between the ketone-only (ΔIVP = 1) and alcohol-only (ΔIVP = 2.2) cases. Therefore, variations in the assumed number of oxygens added per reaction are expected to have a greater influence on the shape of the yield or growth curves than differences in the assumed ΔIVP, as is evident from Fig. 7b.

3.1.4 Oxidation of multi-component mixtures

Only single component SOA precursor reactions have been considered thus far. In the atmosphere, simultaneous oxidation of many different precursors occurs. To assess the generalizability of the single component results, oxidation simulations have been carried out for a mixture of precursor compounds, using $N_C = 15$ to $N_C = 5$. The initial gas-phase concentrations were adjusted such that after 10 h of simulation at $[OH] = 2 \times 10^6$ the total abundance of products from each of the individual precursors were approximately equal (around 0.9 $\mu g\,m^{-3}$ each to give $C_{OA,total} = 10\,\mu g\,m^{-3}$). So that products from individual precursors could be identified c_{frag} was set to zero and for simplicity 1 oxygen was assumed added per reaction. The mean O:C for each group of compounds originating from a specific precursor (i.e., $N_C = 15$ only) was calculated and can be compared with the O:C values obtained from the single-compound simulations. For these specific conditions, the O:C for compounds with $N_C > 13$ were negligibly increased (e.g., 0.157 to 0.163 for $N_C = 15$) while the O:C for smaller compounds decreased slightly (e.g., 1.11 to 1.02 for $N_C = 5$). The differences were slight in all cases, indicating that the single-component results are general.

3.1.5 Ageing, dilution and SOA formation timescales

Given sufficient time or sufficiently high OH concentrations, all of the SOA precursor will react away. At this point it is reactions of the product molecules that lead to continued SOA growth. Once again, the $N_C = 12$ system is considered, but now the calculations are run for 50 days at $[OH] = 2 \times 10^6$ molecules cm^{-3}, still assuming ΔIVP = 1.6,

ACPD
12, 3295–3356, 2012

1 oxygen per reaction and that $C_{OA} = 10\,\mu g\,m^{-3}$ at the end of the simulation. (This is equivalent to ~60 lifetimes of oxidation for an alkane-type $N_C = 12$ precursor. Note that equivalently a higher [OH] and shorter timescale could be used.). With $c_{frag} = 0$, the SOA produced rapidly reaches the maximum yield (by around 3 lifetimes). The mean O:C reaches a minimum of 0.33 around 3 lifetimes, after which it very slowly increases to a plateau at ~0.4 at 60 lifetimes. The increase in O:C is slow because the majority of the available material by that point exists in the particle phase, and thus gas-phase oxidation becomes slow and the particle composition does not change much with time.

If fragmentation is included (with $c_{frag} = 0.2$), somewhat different results are obtained. The C_{OA} peaks and then decreases as, over time, gas-phase reactions convert lower volatility long-chain species into higher volatility short-chain species, thus causing evaporation from the particle phase and decreasing the particle mass. However, some of this evaporated mass reacts and is recycled to the particle phase as higher O:C material leading to a substantial increase in the O:C over time (from 0.35 at the minimum to 0.62 at 60 lifetimes). Now the result expected above is obtained; fragmentation does lead to production of OA with elevated O:C, compared to the no fragmentation case. However, this only occurs after many lifetimes of oxidation, i.e., once >99 % of the SOA precursor hydrocarbon has reacted, which will usually correspond to very long time-scales (days to weeks) in the atmosphere. We therefore still conclude that fragmentation in the gas-phase is generally an inefficient pathway for increasing the O:C of OA.

The large potential variation in O:C above must be reconciled with timescales associated with the production of SOA mass in the atmosphere, where strong SOA production often occurs at relatively short times and close to sources (e.g., Dzepina et al., 2009). (Recall that for a $N_C = 12$ alkane-type hydrocarbon, 1 lifetime is approximately equal to 10 h, or ~1 day of sunlight, of ageing at 2×10^6 molecules cm^{-3}.) Thus, the above calculations, although illustrative, may not have much relation to what occurs in the atmosphere because to limit SOA production to $10\,\mu g\,m^{-3}$ over 60 lifetimes required that the C_{OA} at short lifetimes were very small and at 1 lifetime were almost negligible.

ACPD
12, 3295–3356, 2012

Therefore, similar calculations have been performed where the $[HC]_0$ values were increased so that $C_{OA}(\tau_{OH} = 1) = 1\,\mu g\,m^{-3}$. The calculated O:C still increase over long times, especially with fragmentation included, although by less than the case above (Fig. 8). However, an unrealistically large amount of SOA is now formed at longer lifetimes, up to $100\,\mu g\,m^{-3}$. Such substantial SOA production over long timescales is inconsistent with atmospheric observations, although over such long atmospheric timescales dilution of an airmass with "background" air must be computed.

Calculations have therefore been performed assuming that the gas + particle system is diluted with "background" air (where gas and particle concentrations are assumed zero) at a rate of $5\,\%\,h^{-1}$, but still with $C_{OA}(\tau_{OH} = 1) = 1\,\mu g\,m^{-3}$. Initially the C_{OA} and O:C follow the no-dilution case, but with dilution the C_{OA} peaks around 3 lifetimes (at $C_{OA} \sim 10\,\mu g\,m^{-3}$) and then falls to zero after ~10 lifetimes. (The details depend on the assumed dilution rate, but the general results are independent.) As the C_{OA} decreases, the O:C for both the fragmentation and no-fragmentation cases begin to rise rapidly. This is a result of preferential evaporation and subsequent reaction of the more volatile components that have lower O:C values, and condensation of the higher O:C products, as the system is diluted.

Above, it was assumed that $[OH] = 2 \times 10^6$ molecules cm^{-3}, a typical daytime average value. However, higher OH concentrations are sometimes observed in the atmosphere. When [OH] is increased, the lifetime vs. actual time relationship is modified, with the timescale for oxidation being compressed. For example, at $[OH] = 1x \times 10^7$ molecules cm^{-3}, 2 h ~ 1 lifetime. At this larger OH concentration, the O:C that can be obtained over 1 day is increased somewhat over the smaller OH case because more reactions occur (and thus more oxygen is added). However, although oxidation proceeds faster, dilution will play a less important role because of the shorter timescale (assuming a constant dilution rate), which suppresses the O:C that can be obtained at a given lifetime relative to oxidation at lower OH. Overall, these computational results indicate that ageing and dilution can, in principle, lead to SOA with high O:C. However, noting that these calculations used the smallest N_C IVOC ($N_C = 12$), it

ACPD
12, 3295–3356, 2012

can be generally concluded that over timescales of ~1 day or less it is difficult to form SOA with high O:C (>0.4) from IVOCs and SVOCs, even at high OH.

3.2 SOA volatility vs. O:C

The volatility (i.e., C^*) of the individual compounds comprising the SOA formed can be monitored throughout the reaction. Although lower volatility compounds have a greater propensity to reside in the particle phase, Eq. (3) shows that the absolute abundance of a given compound in the particle phase also depends on the total abundance of that compound. Just because a compound has a relatively high volatility does not mean that it will not exist in the particle phase with significant abundance. The mean $\log C^*$ value of the condensed phase products, weighted by mass, has been computed along with the mean O:C for Case 2B from Sect. 3.1.2 (i.e., $10\,\mu g\,m^{-3}$ formed over 1 lifetime of oxidation, including fragmentation, with $\Delta IVP = 1.6$ and 1 oxygen added per reaction). The trajectory of the OA through the space defined by O:C and $\log C^*$ (Jimenez et al., 2009; Donahue et al., 2011) is shown in Fig. 9. As OA forms, the mean volatility reaches a minimum where the O:C reaches a maximum. However, both occur when only very little OA has formed. The "fishhook" behavior occurs around the point when OA formation begins in earnest (e.g., $C_{OA} > 0.01\,\mu g\,m^{-3}$), which is when more than just the very lowest volatility components begin to contribute in a substantial way (in a similar manner to what was shown in Fig. 3a). Because the system is controlled by gas-particle partitioning, the mean OA volatility never falls much below $\log C^* = 0$. This is because, as already shown, fragmentation does not efficiently lead to the production of significant amounts of low volatility (high O:C) material. For these examples the model is run until $10\,\mu g\,m^{-3}$ has formed so it should not be surprising that the mean $\log C^*$ for all N_C SOA precursors ends up around $10\,\mu g\,m^{-3}$.

ACPD
12, 3295–3356, 2012

3.3 Formation of oxidized organic aerosol

Ambient SOA is a complex mixture of compounds. Factor analysis of ambient OA time-series measurements (Ulbrich et al., 2009; Zhang et al., 2011), coupled with estimates of OA volatility (Huffman et al., 2009a; Cappa and Jimenez, 2010) provide some constraints on the likely range of values for O:C and volatility of ambient SOA. Factor analysis results suggest that SOA can be equated with a general "oxidized" organic aerosol (OOA) factor, which can be further subdivided into "low volatility" and "semi volatile" components (LV-OOA and SV-OOA, respectively), each with distinct properties (Jimenez et al., 2009). Jimenez et al. (2009) suggest a range of likely values for the O:C and log C^* for LV-OOA and SV-OOA (shown in Fig. 9). It is evident that gas-phase reactions, coupled with gas-particle partitioning theory, does not lead to the production of material with sufficiently low volatility so-as to be classified as LV-OOA, and even the SV-OOA category is limited. However, and perhaps more importantly, it is clear that only a small subset of N_C yields SOA with O:C that is consistent with LV-OOA or SV-OOA formation on relatively short time-scales (about 1 day). In the case of SV-OOA, compounds with $8 \leq N_C \leq 11$ are needed. For LV-OOA compounds with $N_C \leq 8$ are needed. Oxidation of the vast majority of IVOC and of all SVOC compounds will not lead to SOA with sufficiently high O:C to match OOA, even when fragmentation is included.

It is possible to shift this range of N_C somewhat by altering the assumed ΔIVP towards lower values, but only within well-defined limits constrained by physical expectations (i.e., it is generally not appropriate to assume $\Delta\text{IVP} < 1$). Additionally, observations suggest that such small ΔIVP values are unlikely, as much ambient OA moves along a line in van Krevelen space (a graph of H:C vs. O:C) that indicates equal addition of alcohols and ketones, or greater addition of alcohol groups (Heald et al., 2010; Ng et al., 2011). Also, as ΔIVP is decreased aerosol yields decrease (cf. Fig. 2), and thus any choice of ΔIVP must be reconciled self-consistently with laboratory observations of aerosol yields.

ACPD
12, 3295–3356, 2012

Previously, highly oxidized (O:C > 0.5) SOA produced from photooxidation of heptadecane (an IVOC with $N_C = 17$) under high-NO_x conditions and low C_{OA} (~2 µg m^{-3}) has been observed (Presto et al., 2009). It was suggested that fragmentation of the heptadecane in the gas-phase and subsequent reaction and condensation of highly oxidized fragments was the likely reason for the formation of the highly oxidized OA. The results from the SOM suggest that this is not a likely mechanism. Presto et al. (2009) used high [OH] (~2×10^7 molecules cm^{-3}) with low precursor concentrations to produce the OA and, by the end of the experiments, the reaction had gone through multiple oxidation lifetimes (~3). We have simulated the general reaction conditions from Presto et al. (2009) and find that the calculated O:C is <0.20, even when fragmentation is included. The reason for this model/measurement discrepancy is unknown. The model results are, however, quantitatively consistent with the O:C observed for low-NO_x, low-C_{OA} experiments presented in the same study (observed O:C = 0.17).

3.4 On the viability of a POA-to-gas-to-SOA pump

Semi-volatile compounds by definition are those that exist with significant abundances in both the gas and particle phases. In the context of partitioning theory, this corresponds to those compounds that have C^* values within an order of magnitude of the total C_{OA}; compounds with C^* values much greater or lower than this will exist predominately in one phase or the other. As semi-volatile compounds are oxidized in the gas-phase, this will shift the partitioning of the semi-volatile OA components towards the gas-phase where they can now be oxidized. After 1 oxidation reaction these semi-volatile compounds likely become sufficiently low volatility to partition strongly back to the particle phase, assuming no fragmentation takes place. This "pumping" mechanism can, in principle, lead to a more oxidized OA being formed but without a significant increase in OA mass (Kroll et al., 2007). There have been some suggestions that this pumping mechanism can explain the evolution of OA in biomass burning plumes as they age (Capes et al., 2008), effectively converting primary organic aerosol (POA) to

ACPD
12, 3295–3356, 2012

SOA (sometimes termed oxidized POA, or OPOA; Miracolo et al., 2010). Note that the SOM inherently includes this pumping mechanism since reactions are assumed to occur solely in the gas-phase and gas-particle equilibrium is assumed throughout.

The importance of this mechanism for increasing aerosol O:C will depend upon a few key factors: (1) the rate of oxidation of the semi-volatile compounds, (2) the rate of formation of SOA from compounds already present in the gas-phase, (3) the volatility of the SOA precursor and (4) the likelihood of fragmentation. Below, a few cases are considered using a single-component system. For illustrative purposes, it will be assumed in all cases that there is some initial POA mass, in equilibrium with the gas-phase, and that the initial $C_{OA} = 10\,\mu g\,m^{-3}$ (the general conclusions hold for any C_{OA}). We will distinguish between OPOA and the total SOA (the sum of OPOA and SOA originating from compounds initially present in the gas-phase) and will designate OA present in the particle-phase at the start of a simulation as POA.

Consider first a compound where $C^* \ll C_{OA}$. A $N_C = 25$ compound has a $C^* \sim 0.5\,\mu g\,m^{-3}$ and thus for $C_{OA} = 10\,\mu g\,m^{-3}$ will be 95 % in the particle phase (leaving only $0.5\,\mu g\,m^{-3}$ in the gas-phase). Within the SOM, the absolute abundance of the SOA precursor is tracked in both the particle and gas phases. Starting from $C_{POA} = 10\,\mu g\,m^{-3}$, after 10 h of oxidation at $[OH] = 2x \times 10^6$ molecules cm^{-3} the C_{POA} has decreased to $9\,\mu g\,m^{-3}$ while the total OA has increased to $10.15\,\mu g\,m^{-3}$. This indicates that only ~10 % of the POA has been converted to OPOA, although the OPOA/SOA ratio is approximately 87 %, indicating that, of the small amount of SOA formed, OPOA is a dominant SOA component. Because the oxidation products only need to go through one reaction with OH before condensing, very little oxygen is added and the O:C will increase by only a very small amount. If fragmentation is included the O:C may increase by a slightly larger amount, but then the ability of the products to condense will be decreased (due to their higher volatilities) and the amount of SOA formed is decreased. If [OH] is increased to 2×10^7 molecules cm^{-3}, the amount of POA evaporated increases to 65 % over 10 h. Overall, if the OA mass is dominated by compounds with $C^* \ll C_{OA}$, the pumping mechanism will be relatively inefficient because a small relative amount of

ACPD
12, 3295–3356, 2012

vapors exists and oxidation of these vapors will only very slowly recycle more oxidized material back into the particle phase.

If the OA mass is instead dominated by compounds with $C^* \sim C_{OA}$ the initial POA material will be ~50/50 partitioned between the gas and particle phases. For $C_{OA} = 10\,\mu g\,m^{-3}$, this corresponds to an N_C ~22 alkane-like hydrocarbon. Now, over 10 h at $[OH] = 2 \times 10^6$ molecules cm^{-3}, ~50 % of the POA mass is lost, suggesting that a fair amount of mass can be transferred through the pumping mechanism. However, there is at the same time formation of $\sim 10\,\mu g\,m^{-3}$ of SOA from material originally in the gas-phase, and thus the OPOA/SOA ratio is only ~1/3. If $[OH] = 2 \times 10^7$ molecules cm^{-3} nearly all the POA is lost, but this still only represents ~40 % of the total SOA mass. This makes sense because the upper-limit contribution of OPOA to the total SOA under these conditions is 50 %.

If the OA mass is dominated by compounds with $C^* = 100\,\mu g\,m^{-3} \gg C_{OA}$ ($N_C \sim 20$), then the gas/particle split will initially be 90/10 at $C_{POA} = 10\,\mu g\,m^{-3}$. Unlike the previous two cases the POA abundance initially increases with oxidation because, as SOA is formed from material originally in the gas-phase, the partitioning of the POA to the particle-phase is increased due to the increase in total OA (= POA + SOA). Eventually the C_{POA} peaks (around 2 h), after which time the C_{POA} decreases as the pumping mechanism begins to compete with the increasing C_{OA}. Also, as with the $C^* = C_{OA}$ case above, there is a significant amount of new SOA formed, and thus only ~10 % or so of the total SOA is OPOA. At $[OH] = 2 \times 10^7$ molecules cm^{-3}, all of the C_{POA}, is lost, but this still only represents <10 % of the total SOA mass (consistent with the initial 90/10 split).

The above examples are single component systems. In a multi-component system (many precursors), the partitioning to the particle phase of any given compound is enhanced (via Raoult's Law) at a given C_{OA}. To assess the importance of having a mixture vs. a single component system, calculations have been run for $C_{POA,initial} = 10\,\mu g\,m^{-3}$ for a mixture of $N_C = 25$, 22 and 20 compounds, assuming that each compound contributes equally to the initial POA mass (i.e., the initial $C_{POA} = 3.33\,\mu g\,m^{-3}$ for each

ACPD
12, 3295–3356, 2012

compound) (Fig. 10). Before approximately 2 lifetimes of oxidation (referenced to the $N_C = 25$ compound k_{OH}), the C_{POA} initially increases for all of the compounds, which indicates that the increase in total OA mass is suppressing the OPOA pump. At longer times, the C_{POA} for the $N_C = 22$ and 20 compounds do decay towards zero and form OPOA, but the C_{POA} for the $N_C = 25$ compound remains approximately constant.

Miracolo et al. (2010) presented observations of the contribution of OPOA to the total OA during oxidation experiments of motor oil and *n*-pentacosane ($N_C = 25$). Using a variety of tracers to deduce the OPOA fraction, they found that the OPOA fraction was significant. Without specific details of the actual distribution of compounds comprising the gas and particle phases in the Miracolo et al. (2010) experiments it is difficult to conduct an explicit simulation for comparison with the motor oil results. However, their experiments were run at [OH] $\sim 2 \times 10^7$ molecules cm^{-3} for 3 h, which corresponds to $\sim$7 oxidation lifetimes. At this point in the simulations shown in Fig. 10 OPOA from the $N_C = 22$ and 20 compounds is significant (as indicated by the decrease in C_{POA} for these compounds), generally consistent with their observations. However, if the motor oil system is approximated by assuming that the POA is comprised of equal abundances of $N_C = 20$, 22 and 25 precursors (with $C_{POA,total} \sim 90\,\mu g\,m^{-3}$, as in Miracolo et al., 2010) the calculated decrease in the total C_{POA} quantitatively follows the decay of their "*m/z* 57" tracer for POA, although the amount of SOA formed is over-predicted (Fig. 11). Given that we do not actually know the initial distribution of compounds and that heterogeneous reactions are not included in the SOM, the model/measurement agreement is reasonable. The experiments run using *n*-pentacosane alone showed much less SOA and OPOA formation (Miracolo et al., 2010), consistent with the general conclusions from the model. Calculations specifically run using the approximate conditions in Miracolo et al. ($C_{POA,initial} = 5\,\mu g\,m^{-3}$, [OH] $= 2 \times 10^7$ molecules cm^{-3}) again show a decrease in the calculated C_{POA} that is quantitatively consistent with the observations, although now the SOA formation is under-predicted at early times and over-predicated at later times.

ACPD
12, 3295–3356, 2012

Of note is the finding that the only simulations in which the total OA mass is conserved as oxidation proceeds is for compounds where $C^* < C_{OA}$. For compounds with $C^* \geq C_{OA}$ significant SOA formation occurs and the total C_{OA} increases substantially with time. However, when $C^* < C_{OA}$, the model indicates that very little mass is actually converted from POA to OPOA, and thus the mean properties of the OA, in particular O:C, will not change substantially, especially so since it is likely only necessary for molecules to undergo 1 reaction before recondensing and only a finite number of oxygens can be added per reaction. It is therefore difficult to substantially change the mean particle intensive properties in the absence of significant SOA formation. If, however, dilution of an air mass occurs concurrent with oxidation (such as in a plume downwind of a biomass burning event), it is possible for the absolute C_{OA} to decrease even in the presence of SOA (and OPOA) formation. Dilution will enhance the chemical pump by causing evaporation of semi-volatile compounds, thus increasing the fractional contribution of OPOA to total SOA, although not negating entirely "traditional" SOA formation. For example, for a single component system with $N_C = 21$ ($C^* = 38\,\mu g\,m^{-3}$) starting with $C_{OA} = 50\,\mu g\,m^{-3}$, simultaneous dilution and reaction (at [OH] = 2x × 10^6 molecules cm^{-3} for 10 h) leads to an approximate linear decrease in C_{OA} when compared with a (fictitious) conserved tracer when dilution rates are ~10 % h^{-1} or greater (Fig. 12), although the OPOA contribution to the total SOA is always <50 %, given the starting conditions. These conditions correspond approximately to those in the study by Capes et al. (2008) where they observed a linear relationship between C_{OA} and CO in a plume evolving downwind of a biomass burning event (although we note that we do not have specific information as to [OH] or dilution rates encountered during that study).

Taken all together, the model results suggest that the gas-phase pumping mechanism will often be relatively inefficient at typical ambient OH concentrations since for semi-volatile compounds with "low" volatility not much mass is transferred through the gas-phase, while for semi-volatile compounds with "high" volatility the SOA formation from vapors already present in the gas-phase dominates. Dilution may serve as a

ACPD
12, 3295–3356, 2012

means to evaporate "low" volatility material at a much faster rate than the chemical pump, and thus may be a mechanism towards significant OPOA production (since the particle phase fraction of these "low" volatility SVOCs is larger than for "high" volatility SVOCs to begin with). Also, if exceptionally high OH concentrations are encountered, the OPOA formation mechanism may contribute to the total SOA burden. Ultimately, the contributions of OPOA to the total SOA burden will depend sensitively on the actual distribution of semi-volatile compounds comprising the initial POA, as well as the abundance of more volatile VOCs that can also form SOA.

4 Two examples

The SOM can be used to compute the time evolution of aerosol mass (or yields) and the mean O:C. By comparing with laboratory aerosol yield experiments, it is possible to constrain the adjustable model parameters to fit the data. Recall that there are three parameters to be tuned: the ΔIVP, the c_{frag} (or m_{frag}) and the number of oxygens added per reaction. (This last term is not strictly a single parameter, but an array of probabilities of adding 1, 2, 3 or 4 oxygen atoms per reaction). Here, two examples are considered: (1) α-pinene photooxidation under low-NO_x conditions (Ng et al., 2006) and (2) pentadecane photooxidation under high-NO_x conditions (Presto et al., 2010). Because α-pinene contains a single double bond, the reaction rate of α-pinene with OH is likely to be faster than that of its oxidation products. To account for this, the k_{OH} matrix has been modified to explicitly assign a value for the reaction of OH with α-pinene ($k_{\mathrm{OH}} = 5.3 \times 10^{-11}$ molecules cm^{-3}; Gill and Hites, 2002), with the rate coefficients of all other products computed using the scheme from Eq. (1).

Ng et al. (2006) measured an aerosol growth curve (C_{OA} vs. f_{HC}) for α-pinene oxidation that can be computed by our model. The model inputs are $[\mathrm{HC}]_0 = 108$ ppb and $[\mathrm{OH}] = 3 \times 10^6$ molecules cm^{-3}. If only a fixed number of oxygens are assumed added per reaction (e.g., 1 or 2), no solution is possible because 1 oxygen per reaction does not form OA fast enough while 4 oxygens forms OA much more rapidly than is

ACPD
12, 3295–3356, 2012

observed in the experiment. A good solution comes from a combination of parameters: ΔIVP = 1.85, c_{frag} = 0.2, and the probability distribution of oxygens added is [1, 2, 3, 4] = 0.20, 0.32, 0.32, 0.16], when small fragments are assumed (Fig. 13). Smaller values of ΔIVP give the wrong curvature while smaller values of c_{frag} lead to an over-prediction of the absolute OA mass. Random fragmentation gives almost the same set of parameters, although with a slightly smaller $c_{frag} \sim 0.19$. (Note that in the random case each time the model is run one obtains a slightly different solution because the fragmentation probabilities are computed using a random number generator. However, the run-to-run variability is relatively small.) Use of Eq. (5) for P_{frag} gives very similar results when $m_{frag} = 0.5$, with ΔIVP = 1.80 and the same oxygen probability distribution as above. If $P_{frag} = (O:C)^{1/6}$ is assumed it is not possible to match the observations for any combination of ΔIVP and the functionalization array. The distribution of particulate-phase compounds in N_C/N_O space with fractional populations >0.01 % is also shown for select points along the simulated reaction (Fig. 13). The distribution of oxidation products evolves throughout the simulation, with compounds of lower N_C, higher N_O contributing more significantly at later times, although at all times contributions of N_C = SOA precursor species dominate.

The validity of these model results can be evaluated in light of what is known about the α-pinene oxidation mechanism. For α-pinene oxidation, the OH addition pathway dominates (90 %), and condensed-phase products with 2, 3 and 4 oxygens have been observed (Larsen et al., 2001; Jaoui and Kamens, 2003). Additionally, some of these products have fewer carbon atoms than α-pinene, indicating that fragmentation does occur. The model distribution of products in carbon/oxygen space can be compared with experimentally detected compound structures. Figure 13 shows that there is generally good agreement between the predicted and observed distribution of compounds (Larsen et al., 2001; Jaoui and Kamens, 2003), although notably a compound with coordinates $N_C = 10$, $N_O = 5$ is predicted to exist but has not, to our knowledge, been previously observed, although it has been suggested as a possible product of α-pinene ozonolysis (Shilling et al., 2009). Additionally, the model predicts an O:C for the OA

ACPD
12, 3295–3356, 2012

of ~0.39, which compares extremely well with observations (O:C = 0.40; Chhabra et al., 2011). This comparison between model and experiment suggests that the statistical representation of oxidation in this system is indeed a good approximation of the chemistry.

For the pentadecane system (Presto et al., 2010), the temporal evolution of the C_{OA} can be used for tuning the model parameters (cf. their Fig. 1). For this experiment, OH was not constant, and thus OH in the model is allowed to change so that the temporal behavior of the measured pentadecane concentrations can be replicated. Excellent model/measurement agreement is obtained for ΔIVP = 1.85 and c_{frag} = 0.33 (Eq. 4) with the probability distribution of oxygens added as [1, 2, 3, 4] = [0.45, 0.55, 0.0, 0.0] or for ΔIVP = 1.82, m_{frag} = 0.33 (Eq. 5) and [0.39, 0.61, 0.0, 0.0] (Fig. 14). Both these and the α-pinene results above indicate that the selected functional form for P_{frag} does not strongly influence the results, so long as the tunable parameters (c_{frag} or m_{frag}) are set appropriately. The evolution of the particle-phase N_C/N_O molecule distributions are also shown at selected points during the reaction, and indicate that the particle composition is continuously evolving. Although the ΔIVP is identical to the α-pinene system, the fragmentation probability is increased and now only 1 and 2 oxygens are added per reaction. The latter can be understood by recognizing that, without a double bond, oxidation of dodecane proceeds via hydrogen abstraction and is likely to add fewer oxygen atoms per reaction. The somewhat larger fragmentation probability may be related to the high-NO_x vs. low-NO_x conditions or possibly the cyclic structure of α-pinene, which if carbon bonds are broken can leave the total number of carbons in the molecule intact (i.e., ring-opening).

The model predicts an O:C of 0.14. Presto et al. (2010) do not directly report O:C, but they do report the fraction of the aerosol mass spectrum at *m/z* 44 (f_{44}), which has been previously shown to have a relationship to O:C (Aiken et al., 2008; Sun et al., 2009). Using the f_{44} vs. O:C relationship, the O:C for the high-NO_x pentadecane OA is estimated to be ~0.20, although it should be noted that the f_{44} for pentadecane OA is lower than the measurement range in both these papers and, from the data shown in

ACPD
12, 3295–3356, 2012

Aiken et al. (2008), there is reason to suspect that this relationship may over-estimate O:C at lower f_{44} (cf. the "AMB_{ground}" and "HOA_{ground}" points in their Fig. 4). Given this uncertainty, the level of agreement between model and experiment is satisfactory. Nonetheless, it is clear that the multi-generational model developed here provides a robust framework for modeling the formation and evolution of SOA.

5 Implications and conclusions

The development of a kinetic, statistical model of SOA formation that accounts for the multi-generational addition of oxygen, fragmentation and volatility within the general framework of gas-particle partitioning theory, termed the statistical oxidation model, has been presented. Results from the SOM indicate that the particle-phase O:C is primarily controlled by the number of carbons comprising the gas-phase SOA precursor, when only gas-phase processing is considered. Specifically, the model results indicate that gas-phase processing of SVOC's and IVOC's produces SOA with O:C < 0.4 or O:C < 0.2, respectively, even after multiple days of ageing. These results suggest that it is not possible to simultaneously have IVOCs and SVOCs contribute significantly to the total SOA mass and to have a high average particle O:C, at least when only gas-phase processes are considered. Importantly, this conclusion remains unchanged even when fragmentation is included in a physically plausible manner. This is a consequence of the strong relationship between the number of oxygen-containing functional groups, N_C and volatility. For a given N_C compound, there is effectively a cap on the O:C for SOA. Gas-phase mechanisms have been shown unable to form "OOA", in particular because of the difficulty of forming compounds with sufficiently low volatility. In the case of IVOCs and SVOCs, this conclusion is also related to the difficulty of forming sufficiently oxidized OA on the required time-scales. Fragmentation has been shown to be an important aspect of the SOA formation process and has a strong influence on the aerosol yield.

ACPD
12, 3295–3356, 2012

The recent push towards model development that incorporates tracking of average particle properties, such as O:C and volatility, in addition to the extensive property C_{OA} is useful, as it helps to constrain models that in terms of whether the fundamental processes governing SOA formation are being represented realistically. However, care must be taken because it is possible to construct models with physically unrealistic composition/volatility relationships that can yield results that appear to match observations (e.g., Hodzic et al., 2010; Dzepina et al., 2011; Murphy et al., 2011). (For example, an assumption of an increase in mass by 40 % per reaction due to oxygen addition, as in these studies, corresponds to an addition of ~5 oxygens per reaction for a C_{15} hydrocarbon but only 3 oxygens per reaction for a C_9 hydrocarbon. If this is assumed to correspond to the same change in C^* per reaction for both species (e.g., 2 orders of magnitude), this suggests that the reaction pathways for these two molecules provide fundamentally different ΔIVP per oxygen relationships, corresponding to ΔIVP = 0.4 or ΔIVP = 0.7 for C_{15} and C_9, respectively, both of which are much lower than what is physically likely. Assuming instead a mass increase of 7.5 % per reaction with a decrease in C^* of 1 order of magnitude corresponds to the addition of 1 and 0.6 oxygens per reaction and ΔIVP = 1 and ΔIVP = 1.7 for C_{15} and C_9, respectively.) Additionally, multi-generational oxidation of "traditional" SOA precursor species should be incorporated into models (Tsimpidi et al., 2010; Dzepina et al., 2011), as opposed to static yield approaches that assume that products do not react. In particular, it is not appropriate to exclude such species (e.g., toluene, α-pinene) from multi-generational oxidation schemes while including IVOC and SVOC species (e.g., Shrivastava et al., 2011). To do so unfairly increases the aerosol yields from IVOC and SVOC species over traditional species, especially on long timescales (e.g., multiple days of ageing). For example, Dzepina et al. (2011) found that if both IVOC/SVOC and traditional VOC species are allowed to age for 3 days (i.e., undergo multi-generation oxidation) the ratio between the SOA mass formed from IVOC/SVOC and traditional VOCs is is ~1.2, whereas if only IVOC/SVOC species are allowed to age while traditional VOCs are assumed to have static yields the ratio is ~7.

ACPD
12, 3295–3356, 2012

To reconcile our model results with observations that indicate much SOA has both high O:C and low-volatility suggests a few, potentially overlapping, possibilities:

1. IVOCs and SVOCs do not contribute substantially to the SOA burden. If these compounds comprised a significant fraction of the total OA mass, it would be very difficult to obtain mean O:C values as high as have been observed in the atmosphere (Aiken et al., 2008; Ng et al., 2011).

2. Compounds with relatively small N_C are the predominant SOA precursors in the atmosphere (to obtain a high O:C) and condensed-phase oligomerization reactions readily occur (to lower the volatility).

3. Condensed or aqueous phase reactions that add oxygen occur on relatively rapid time scales. This would increase O:C and decrease volatility. This case is distinct from oligomerization reactions since the latter do not often lead to oxygen addition and typical heterogeneous reactions with OH are too slow.

4. Contributions to OA mass from small oxygenates with very high O:C, such as glyoxal (Ervens and Volkamer, 2010; Ervens et al., 2011), are more important than is sometimes recognized. Note that if IVOCs and SVOCs (and other VOCs) are the precursors of these small oxygenates formed by fragmentation, they may be the proximate source of the OA mass, but not in the manner traditionally imagined.

5. Equilibrium partitioning theory does not provide an adequate description of much atmospheric OA, possibly due to the conversion of OA to a non-absorbing phase (Cappa and Wilson, 2011; Koop et al., 2011; Vaden et al., 2011).

That the volatility of model SOA is substantially higher than that of ambient OA (Cappa and Jimenez, 2010) suggests that condensed phase reactions may play a key role. Such reactions may or may not involve the aerosol aqueous phase. If condensed phase reactions simply lead to oligomerization of already condensed mass, then the originating compounds must be small ($N_C < 10$) in order to form OA with sufficiently

ACPD
12, 3295–3356, 2012

high O:C (point 2 above). Such oligomerization reactions are a likely explanation for the apparently low volatility of chamber SOA, independent of N_C and O:C (although chamber SOA is often still more volatile than ambient OA; Huffman et al., 2009b). However, if the condensed phase reactions occur that actually add oxygen (point 3), such as oxidation of phenolic compounds in aqueous solutions (Sun et al., 2010), then in principle compounds with any N_C may contribute to SOA (although such reactions are likely to involve aromatic compounds that have relatively small N_C to begin with).

SOA chamber experiments have traditionally been parameterized in terms of the volatility and yield of specific products, whether the classic 2-product model (Odum et al., 1996) or the volatility basis set (VBS) model (Donahue et al., 2006). However, these frameworks do not easily lend themselves to consideration of multi-generational oxidation. In fact, the very exercise of fitting an aerosol yield curve to extract the traditional parameters (C^* and yield for the 2-product model, or just yield for the VBS) has an implicit assumption that products do not react and the yield of each product is static. As shown in Fig. 6, the yields of various products are dynamic and evolve statistically throughout the oxidation process. Extensions of these models after the fact to account for multi-generational oxidation will therefore not truly capture the dynamic evolution of the system because they consider the oxidation of products that were originally derived without consideration of kinetics and the multi-generation aspect of oxidation via OH. (These comments do not necessarily apply to O_3 oxidation experiments for compounds with a single double bond. However, consideration of the continued oxidation of the "first-generation" products of such reactions will fall into a similar trap.)

The SOM is inherently a kinetic, multi-generational formulation of the same problem (OA formation) that intrinsically accounts for the evolution of the system with time. This is particularly important to evaluate whether gas-phase oxidation and traditional partitioning theory can explain the rapid time-scale for the formation of highly oxygenated SOA. The tunable parameters derived here can be considered as analogs of the traditional yield/volatility parameters, but contain within them important information about the kinetics, in particular the role of fragmentation. This is not to say that models, such

ACPD
12, 3295–3356, 2012

as the 1 or 2-D VBS, cannot be formulated in a similar manner as ours (e.g., Robinson et al., 2007; Shrivastava et al., 2008; Dzepina et al., 2009; Farina et al., 2010; Hodzic et al., 2010; Murphy et al., 2011), only that the parameters typically extracted from a non-kinetic VBS fit to chamber experiments will not provide the necessary information. Because the distribution of molecules in the SOM is framed as a matrix of oxygen and carbon atoms, it provides a natural framework for the simulation of multi-generational oxidation, including fragmentation. The simultaneous oxidation of multiple compounds can be easily incorporated within the modeling framework simply by adding precursors to the appropriate N_C/N_O cell. Furthermore, one can envision future developments that, for example, include an "oligomerization" operator to account for condensed phase accretion reactions, the role of heterogeneous oxidation (e.g., Smith et al., 2009), or the conversion of OA to a non-absorbing "glassy" phase (Cappa and Wilson, 2011).

Acknowledgements. The authors thank Jesse Kroll (MIT), Kelly Daumit (MIT) and John Seinfeld (Caltech) for useful discussions. This work was funded by the US National Science Foundation (CDC) and by the Director, Office of Energy Research, Office of Basic Energy Sciences, Chemical Sciences Division of the US Department of Energy under Contract No. DE-AC02-05CH11231 (KRW).

References

Aiken, A. C., Decarlo, P. F., Kroll, J. H., Worsnop, D. R., Huffman, J. A., Docherty, K. S., Ulbrich, I. M., Mohr, C., Kimmel, J. R., Sueper, D., Sun, Y., Zhang, Q., Trimborn, A., Northway, M., Ziemann, P. J., Canagaratna, M. R., Onasch, T. B., Alfarra, M. R., Prevot, A. S. H., Dommen, J., Duplissy, J., Metzger, A., Baltensperger, U., and Jimenez, J. L.: O/C and OM/OC ratios of primary, secondary, and ambient organic aerosols with high-resolution time-of-flight aerosol mass spectrometry, Environ. Sci. Technol., 42, 4478–4485, doi:10.1021/es703009q, 2008.

Atkinson, R.: Kinetics of the gas-phase reactions of OH radicals with alkanes and cycloalkanes, Atmos. Chem. Phys., 3, 2233–2307, doi:10.5194/acp-3-2233-2003, 2003.

Aumont, B., Szopa, S., and Madronich, S.: Modelling the evolution of organic carbon during its gas-phase tropospheric oxidation: development of an explicit model based on a self generating approach, Atmos. Chem. Phys., 5, 2497–2517, doi:10.5194/acp-5-2497-2005, 2005.

ACPD
12, 3295–3356, 2012

Barsanti, K. C., Smith, J. N., and Pankow, J. F.: Application of the np+mP modeling approach for simulating secondary organic particulate matter formation from α-pinene oxidation, Atmos. Environ., 45, 6812–6819, doi:10.1016/j.atmosenv.2011.01.038, 2011.

Capes, G., Johnson, B., McFiggans, G., Williams, P. I., Haywood, J., and Coe, H.: Aging of biomass burning aerosols over West Africa: Aircraft measurements of chemical composition, microphysical properties, and emission ratios, J. Geophys. Res., 113, D00C15, doi:10.1029/2008jd009845, 2008.

Cappa, C. D. and Jimenez, J. L.: Quantitative estimates of the volatility of ambient organic aerosol, Atmos. Chem. Phys., 10, 5409–5424, doi:10.5194/acp-10-5409-2010, 2010.

Cappa, C. D. and Wilson, K. R.: Evolution of organic aerosol mass spectra upon heating: implications for OA phase and partitioning behavior, Atmos. Chem. Phys., 11, 1895–1911, doi:10.5194/acp-11-1895-2011, 2011.

Cappa, C. D., Lovejoy, E. R., and Ravishankara, A. R.: Determination of Evaporation Rates and Vapor Pressures of Very Low Volatility Compounds: A Study of the C4–C10 and C12 Dicarboxylic Acids, J. Phys. Chem. A, 111, 3099–3109, 2007.

Cappa, C. D., Lovejoy, E. R., and Ravishankara, A. R.: Evaporation Rates and Vapor Pressures of the Even-Numbered C8–C18 Monocarboxylic Acids, J. Phys. Chem. A, 112, 3959–3964, 2008.

Chhabra, P. S., Ng, N. L., Canagaratna, M. R., Corrigan, A. L., Russell, L. M., Worsnop, D. R., Flagan, R. C., and Seinfeld, J. H.: Elemental composition and oxidation of chamber organic aerosol, Atmos. Chem. Phys., 11, 8827–8845, doi:10.5194/acp-11-8827-2011, 2011.

de Gouw, J. A., Middlebrook, A. M., Warneke, C., Goldan, P. D., Kuster, W. C., Roberts, J. M., Fehsenfeld, F. C., Worsnop, D. R., Canagaratna, M. R., Pszenny, A. A. P., Keene, W. C., Marchewka, M., Bertman, S. B., and Bates, T. S.: Budget of organic carbon in a polluted atmosphere: Results from the New England Air Quality Study in 2002, J. Geophys. Res., 110, D16305, doi:10.1029/2004JD005623, 2005.

Donahue, N. M., Robinson, A. L., Stanier, C. O., and Pandis, S. N.: Coupled partitioning, dilution, and chemical aging of semivolatile organics, Environ. Sci. Technol., 40, 2635–2643, 2006.

Donahue, N. M., Epstein, S. A., Pandis, S. N., and Robinson, A. L.: A two-dimensional volatility basis set: 1. organic-aerosol mixing thermodynamics, Atmos. Chem. Phys., 11, 3303–3318, doi:10.5194/acp-11-3303-2011, 2011.

Dzepina, K., Volkamer, R. M., Madronich, S., Tulet, P., Ulbrich, I. M., Zhang, Q., Cappa,

ACPD
12, 3295–3356, 2012

C. D., Ziemann, P. J., and Jimenez, J. L.: Evaluation of recently-proposed secondary organic aerosol models for a case study in Mexico City, Atmos. Chem. Phys., 9, 5681–5709, doi:10.5194/acp-9-5681-2009, 2009.

Dzepina, K., Cappa, C. D., Volkamer, R. M., Madronich, S., DeCarlo, P. F., Zaveri, R. A., and Jimenez, J. L.: Modeling the Multiday Evolution and Aging of Secondary Organic Aerosol During MILAGRO 2006, Environ. Sci. Technol., 45, 3496–3503, doi:10.1021/es103186f, 2011.

Ervens, B. and Volkamer, R.: Glyoxal processing by aerosol multiphase chemistry: towards a kinetic modeling framework of secondary organic aerosol formation in aqueous particles, Atmos. Chem. Phys., 10, 8219–8244, doi:10.5194/acp-10-8219-2010, 2010.

Ervens, B., Turpin, B. J., and Weber, R. J.: Secondary organic aerosol formation in cloud droplets and aqueous particles (aqSOA): a review of laboratory, field and model studies, Atmos. Chem. Phys., 11, 11069–11102, doi:10.5194/acp-11-11069-2011, 2011.

Farina, S. C., Adams, P. J., and Pandis, S. N.: Modeling global secondary organic aerosol formation and processing with the volatility basis set: Implications for anthropogenic secondary organic aerosol, J. Geophys. Res., 115, D09202, doi:10.1029/2009jd013046, 2010.

Gill, K. J. and Hites, R. A.: Rate Constants for the Gas-Phase Reactions of the Hydroxyl Radical with Isoprene, α- and β-Pinene, and Limonene as a Function of Temperature, J. Phys. Chem. A, 106, 2538–2544, doi:10.1021/jp013532q, 2002.

Grieshop, A. P., Logue, J. M., Donahue, N. M., and Robinson, A. L.: Laboratory investigation of photochemical oxidation of organic aerosol from wood fires 1: measurement and simulation of organic aerosol evolution, Atmos. Chem. Phys., 9, 1263–1277, doi:10.5194/acp-9-1263-2009, 2009.

Heald, C. L., Jacob, D. J., Park, R. J., Russell, L. M., Huebert, B. J., Seinfeld, J. H., Liao, H., and Weber, R. J.: A large organic aerosol source in the free troposphere missing from current models, Geophys. Res. Lett., 32, L18809, doi:18810.11029/12005GL023831, 2005.

Heald, C. L., Kroll, J. H., Jimenez, J. L., Docherty, K. S., DeCarlo, P. F., Aiken, A. C., Chen, Q., Martin, S. T., Farmer, D. K., and Artaxo, P.: A simplified description of the evolution of organic aerosol composition in the atmosphere, Geophys. Res. Lett., 37, L08803, doi:10.1029/2010gl042737, 2010.

Hodzic, A., Jimenez, J. L., Madronich, S., Canagaratna, M. R., DeCarlo, P. F., Kleinman, L., and Fast, J.: Modeling organic aerosols in a megacity: potential contribution of semi-volatile and intermediate volatility primary organic compounds to secondary organic aerosol formation,

ACPD
12, 3295–3356, 2012

Atmos. Chem. Phys., 10, 5491–5514, doi:10.5194/acp-10-5491-2010, 2010.
Huffman, J. A., Docherty, K. S., Aiken, A. C., Cubison, M. J., Ulbrich, I. M., DeCarlo, P. F., Sueper, D., Jayne, J. T., Worsnop, D. R., Ziemann, P. J., and Jimenez, J. L.: Chemically-resolved aerosol volatility measurements from two megacity field studies, Atmos. Chem. Phys., 9, 7161–7182, doi:10.5194/acp-9-7161-2009, 2009a.
Huffman, J. A., Docherty, K. S., Mohr, C., Cubison, M. J., Ulbrich, I. M., Ziemann, P. J., Onasch, T. B., and Jimenez, J. L.: Chemically-Resolved volatility measurments of organic aerosol from different sources, Environ. Sci. Technol., 43, 5351–5357, doi:10.1021/es803539d, 2009b.
IPCC: Climate Change: The Physical Science Basis – Contribution of Working Group I to the Fourth Assessment Report of the Intergovernmental Panel on Climate Change, edited by: Solomon, S., Qin, D., and Manning, M., Cambridge University Press, Cambridge, 996 pp., 2007.
Jacobson, M. C., Hansson, H. C., Noone, K. J., and Charlson, R. J.: Organic atmospheric aerosols: Review and state of the science, Rev. Geophys., 38, 267–294, 2000.
Jaoui, M. and Kamens, R. M.: Gaseous and Particulate Oxidation Products Analysis of a Mixture of α-pinene + β-pinene/O_3 Air in the Absence of Light and α-pinene + β-pinene/NO_x Air in the Presence of Natural Sunlight, J. Atmos. Chem., 44, 259–297, doi:10.1023/a:1022977427523, 2003.
Jathar, S. H., Farina, S. C., Robinson, A. L., and Adams, P. J.: The influence of semi-volatile and reactive primary emissions on the abundance and properties of global organic aerosol, Atmos. Chem. Phys., 11, 7727–7746, doi:10.5194/acp-11-7727-2011, 2011.
Jimenez, J. L., Canagaratna, M. R., Donahue, N. M., Prevot, A. S. H., Zhang, Q., Kroll, J. H., DeCarlo, P. F., Allan, J. D., Coe, H., Ng, N. L., Aiken, A. C., Docherty, K. S., Ulbrich, I. M., Grieshop, A. P., Robinson, A. L., Duplissy, J., Smith, J. D., Wilson, K. R., Lanz, V. A., Hueglin, C., Sun, Y. L., Tian, J., Laaksonen, A., Raatikainen, T., Rautiainen, J., Vaattovaara, P., Ehn, M., Kulmala, M., Tomlinson, J. M., Collins, D. R., Cubison, M. J., Dunlea, E. J., Huffman, J. A., Onasch, T. B., Alfarra, M. R., Williams, P. I., Bower, K., Kondo, Y., Schneider, J., Drewnick, F., Borrmann, S., Weimer, S., Demerjian, K., Salcedo, D., Cottrell, L., Griffin, R., Takami, A., Miyoshi, T., Hatakeyama, S., Shimono, A., Sun, J. Y., Zhang, Y. M., Dzepina, K., Kimmel, J. R., Sueper, D., Jayne, J. T., Herndon, S. C., Trimborn, A. M., Williams, L. R., Wood, E. C., Middlebrook, A. M., Kolb, C. E., Baltensperger, U., and Worsnop, D. R.: Evolution of Organic Aerosols in the Atmosphere, Science, 326, 1525–1529, doi:10.1126/science.1180353,

ACPD
12, 3295–3356, 2012

2009.
Johnson, D., Utembe, S. R., Jenkin, M. E., Derwent, R. G., Hayman, G. D., Alfarra, M. R., Coe, H., and McFiggans, G.: Simulating regional scale secondary organic aerosol formation during the TORCH 2003 campaign in the southern UK, Atmos. Chem. Phys., 6, 403–418, doi:10.5194/acp-6-403-2006, 2006.
Jordan, C. E., Ziemann, P. J., Griffin, R. J., Lim, Y. B., Atkinson, R., and Arey, J.: Modeling SOA formation from OH reactions with C8–C17 *n*-alkanes, Atmos. Environ., 42, 8015–8026, doi:10.1016/j.atmosenv.2008.06.017, 2008.
Kanakidou, M., Seinfeld, J. H., Pandis, S. N., Barnes, I., Dentener, F. J., Facchini, M. C., Van Dingenen, R., Ervens, B., Nenes, A., Nielsen, C. J., Swietlicki, E., Putaud, J. P., Balkanski, Y., Fuzzi, S., Horth, J., Moortgat, G. K., Winterhalter, R., Myhre, C. E. L., Tsigaridis, K., Vignati, E., Stephanou, E. G., and Wilson, J.: Organic aerosol and global climate modelling: a review, Atmos. Chem. Phys., 5, 1053–1123, doi:10.5194/acp-5-1053-2005, 2005.
Koop, T., Bookhold, J., Shiraiwa, M., and Pöschl, U.: Glass transition and phase state of organic compounds: dependency on molecular properties and implications for secondary organic aerosols in the atmosphere, Phys. Chem. Chem. Phys., 13, 19238–19255, 2011.
Kroll, J. H., Chan, A. W. H., Ng, N. L., Flagan, R. C., and Seinfeld, J. H.: Reactions of Semivolatile Organics and Their Effects on Secondary Organic Aerosol Formation, Environ. Sci. Technol., 41, 3545–3550, 2007.
Kroll, J. H., Donahue, N. M., Jimenez, J. L., Kessler, S. H., Canagaratna, M. R., Wilson, K. R., Altieri, K. E., Mazzoleni, L. R., Wozniak, A. S., Bluhm, H., Mysak, E. R., Smith, J. D., Kolb, C. E., and Worsnop, D. R.: Carbon oxidation state as a metric for describing the chemistry of atmospheric organic aerosol, Nat. Chem., 3, 133–139, 2011.
Kwok, E. S. C. and Atkinson, R.: Estimation of hydroxyl radical reaction rate constants for gas-phase organic compounds using a structure-reactivity relationship: An update, Atmos. Environ., 29, 1685–1695, doi:10.1016/1352-2310(95)00069-b, 1995.
Lane, T. E., Donahue, N. M., and Pandis, S. N.: Simulating secondary organic aerosol formation using the volatility basis-set approach in a chemical transport model, Atmos. Environ., 42, 7439–7451, doi:10.1016/j.atmosenv.2008.06.026, 2008.
Larsen, B. R., Di Bella, D., Glasius, M., Winterhalter, R., Jensen, N. R., and Hjorth, J.: Gas-phase OH oxidation of monoterpenes: Gaseous and particulate products, J. Atmos. Chem., 38, 231–276, 2001.
Lee, A., Goldstein, A. H., Kroll, J. H., Ng, N. L., Varutbangkul, V., Flagan, R. C., and Seinfeld, J.

ACPD
12, 3295–3356, 2012

H.: Gas-phase products and secondary aerosol yields from the photooxidation of 16 different terpenes, J. Geophys. Res., 111, D17305, doi:10.1029/2006jd007050, 2006.

Liang, C. and Pankow, J. F.: Gas/Particle Partitioning of Organic Compounds to Environmental Tobacco Smoke: Partition Coefficient Measurements by Desorption and Comparison to Urban Particulate Material, Environ. Sci. Technol., 30, 2800–2805, doi:10.1021/es960050x, 1996.

Lide, D. R. and Kehiaian, H. V.: CRC handbook of thermophysical and thermochemical data, CRC Press, Boca Raton, 518 pp., 1994.

Matsui, H., Koike, M., Takegawa, N., Kondo, Y., Griffin, R. J., Miyazaki, Y., Yokouchi, Y., and Ohara, T.: Secondary organic aerosol formation in urban air: Temporal variations and possible contributions from unidentified hydrocarbons, J. Geophys. Res., 114, D04201, doi:10.1029/2008jd010164, 2009.

Miracolo, M. A., Presto, A. A., Lambe, A. T., Hennigan, C. J., Donahue, N. M., Kroll, J. H., Worsnop, D. R., and Robinson, A. L.: Photo-Oxidation of Low-Volatility Organics Found in Motor Vehicle Emissions: Production and Chemical Evolution of Organic Aerosol Mass, Environ. Sci. Technol., 44, 1638–1643, do:10.1021/es902635c, 2010.

Murphy, B. N., Donahue, N. M., Fountoukis, C., and Pandis, S. N.: Simulating the oxygen content of ambient organic aerosol with the 2D volatility basis set, Atmos. Chem. Phys., 11, 7859–7873, doi:10.5194/acp-11-7859-2011, 2011.

Ng, N. L., Kroll, J. H., Keywood, M. D., Bahreini, R., Varutbangkul, V., Flagan, R. C., Seinfeld, J. H., Lee, A., and Goldstein, A. H.: Contribution of first- versus second-generation products to secondary organic aerosols formed in the oxidation of biogenic hydrocarbons, Environ. Sci. Technol., 40, 2283–2297, 2006.

Ng, N. L., Kroll, J. H., Chan, A. W. H., Chhabra, P. S., Flagan, R. C., and Seinfeld, J. H.: Secondary organic aerosol formation from m-xylene, toluene, and benzene, Atmos. Chem. Phys., 7, 3909–3922, doi:10.5194/acp-7-3909-2007, 2007.

Ng, N. L., Canagaratna, M. R., Jimenez, J. L., Chhabra, P. S., Seinfeld, J. H., and Worsnop, D. R.: Changes in organic aerosol composition with aging inferred from aerosol mass spectra, Atmos. Chem. Phys., 11, 6465–6474, doi:10.5194/acp-11-6465-2011, 2011.

Odum, J. R., Hoffmann, T., Bowman, F., Collins, D., Flagan, R. C., and Seinfeld, J. H.: Gas/particle partitioning and secondary organic aerosol yields, Environ. Sci. Technol., 30, 2580–2585, 1996.

Pankow, J. F.: An Absorption-Model of the Gas Aerosol Partitioning Involved in the Formation

ACPD
12, 3295–3356, 2012

of Secondary Organic Aerosol, Atmos. Environ., 28, 189–193, 1994.
Pankow, J. F. and Asher, W. E.: SIMPOL.1: a simple group contribution method for predicting vapor pressures and enthalpies of vaporization of multifunctional organic compounds, Atmos. Chem. Phys., 8, 2773–2796, doi:10.5194/acp-8-2773-2008, 2008.
Pankow, J. F. and Barsanti, K. C.: The carbon number-polarity grid: A means to manage the complexity of the mix of organic compounds when modeling atmospheric organic particulate matter, Atmos. Environ., 43, 2829–2835, doi:10.1016/j.atmosenv.2008.12.050, 2009.
Presto, A. A., Miracolo, M. A., Kroll, J. H., Worsnop, D. R., Robinson, A. L., and Donahue, N. M.: Intermediate-Volatility Organic Compounds: A Potential Source of Ambient Oxidized Organic Aerosol, Environ. Sci. Technol., 43, 4744–4749, doi:10.1021/es803219q, 2009.
Presto, A. A., Miracolo, M. A., Donahue, N. M., and Robinson, A. L.: Secondary Organic Aerosol Formation from High-NO_x Photo-Oxidation of Low Volatility Precursors: n-Alkanes, Environ. Sci. Technol., 44, 2029–2034, doi:10.1021/es903712r, 2010.
Robinson, A. L., Donahue, N. M., Shrivastava, M. K., Weitkamp, E. A., Sage, A. M., Grieshop, A. P., Lane, T. E., Pierce, J. R., and Pandis, S. N.: Rethinking organic aerosols: Semivolatile emissions and photochemical aging, Science, 315, 1259–1262, 2007.
Russell, L. M., Bahadur, R., and Ziemann, P. J.: Identifying organic aerosol sources by comparing functional group composition in chamber and atmospheric particles, P. Natl. Acad. Sci., 108, 3516–3521, doi:10.1073/pnas.1006461108, 2011.
Seinfeld, J. H. and Pankow, J. F.: Organic atmospheric particulate material, Annu. Rev. Phys. Chem., 54, 121–140, 2003.
Shilling, J. E., Chen, Q., King, S. M., Rosenoern, T., Kroll, J. H., Worsnop, D. R., DeCarlo, P. F., Aiken, A. C., Sueper, D., Jimenez, J. L., and Martin, S. T.: Loading-dependent elemental composition of a-pinene SOA particles, Atmos. Chem. Phys., 9, 771–782, doi:10.5194/acp-9-771-2009, 2009.
Shrivastava, M., Fast, J., Easter, R., Gustafson Jr., W. I., Zaveri, R. A., Jimenez, J. L., Saide, P., and Hodzic, A.: Modeling organic aerosols in a megacity: comparison of simple and complex representations of the volatility basis set approach, Atmos. Chem. Phys., 11, 6639–6662, doi:10.5194/acp-11-6639-2011, 2011.
Shrivastava, M. K., Lane, T. E., Donahue, N. M., Pandis, S. N., and Robinson, A. L.: Effects of gas particle partitioning and aging of primary emissions on urban and regional organic aerosol concentrations, J. Geophys. Res., 113, D18301, doi:10.1029/2007jd009735, 2008.
Smith, J. D., Kroll, J. H., Cappa, C. D., Che, D. L., Liu, C. L., Ahmed, M., Leone, S. R.,

ACPD
12, 3295–3356, 2012

Worsnop, D. R., and Wilson, K. R.: The heterogeneous reaction of hydroxyl radicals with sub-micron squalane particles: a model system for understanding the oxidative aging of ambient aerosols, Atmos. Chem. Phys., 9, 3209–3222, doi:10.5194/acp-9-3209-2009, 2009.

Sun, Y., Zhang, Q., Macdonald, A. M., Hayden, K., Li, S. M., Liggio, J., Liu, P. S. K., Anlauf, K. G., Leaitch, W. R., Steffen, A., Cubison, M., Worsnop, D. R., van Donkelaar, A., and Martin, R. V.: Size-resolved aerosol chemistry on Whistler Mountain, Canada with a high-resolution aerosol mass spectrometer during INTEX-B, Atmos. Chem. Phys., 9, 3095–3111, doi:10.5194/acp-9-3095-2009, 2009.

Sun, Y. L., Zhang, Q., Anastasio, C., and Sun, J.: Insights into secondary organic aerosol formed via aqueous-phase reactions of phenolic compounds based on high resolution mass spectrometry, Atmos. Chem. Phys., 10, 4809–4822, doi:10.5194/acp-10-4809-2010, 2010.

Tsimpidi, A. P., Karydis, V. A., Zavala, M., Lei, W., Molina, L., Ulbrich, I. M., Jimenez, J. L., and Pandis, S. N.: Evaluation of the volatility basis-set approach for the simulation of organic aerosol formation in the Mexico City metropolitan area, Atmos. Chem. Phys., 10, 525–546, doi:10.5194/acp-10-525-2010, 2010.

Ulbrich, I. M., Canagaratna, M. R., Zhang, Q., Worsnop, D. R., and Jimenez, J. L.: Interpretation of organic components from Positive Matrix Factorization of aerosol mass spectrometric data, Atmos. Chem. Phys., 9, 2891–2918, doi:10.5194/acp-9-2891-2009, 2009.

Vaden, T. D., Imre, D., Beránek, J., Shrivastava, M., and Zelenyuk, A.: Evaporation kinetics and phase of laboratory and ambient secondary organic aerosol, P. Natl. Acad. Sci., 108, 2190–2195, doi:10.1073/pnas.1013391108, 2011.

Volkamer, R., Jimenez, J. L., San Martini, F., Dzepina, K., Zhang, Q., Salcedo, D., Molina, L. T., Worsnop, D. R., and Molina, M. J.: Secondary organic aerosol formation from anthropogenic air pollution: Rapid and higher than expected, Geophys. Res. Lett., 33, L17811, doi:10.1029/2006GL026899, 2006.

Wilson, K. R., Smith, J. D., Kessler, S. H., and Kroll, J. H.: The statistical evolution of multiple generations of oxidation products in the photochemical aging of chemically reduced organic aerosol, Phys. Chem. Chem. Phys., 14, 1468–1479, 2012.

Zhang, Q., Jimenez, J. L., Canagaratna, M. R., Ulbrich, I. M., Ng, N. L., Worsnop, D. R., and Sun, Y. L.: Understanding atmospheric organic aerosols via factor analysis of aerosol mass spectrometry: a review, Anal. Bioanal. Chem., 401, 3045–3067, doi:10.1007/s00216-011-5355-y, 2011.

ACPD
12, 3295–3356, 2012

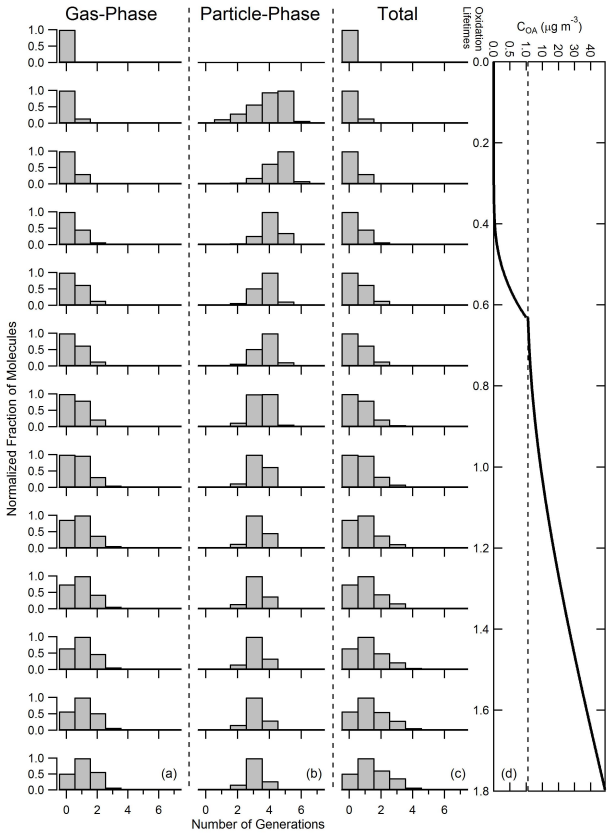

Fig. 1. The time-evolution of gas **(a)**, particle **(b)** and total **(c)** distributions upon reaction of a generic hydrocarbon with OH, normalized to the maximum abundance at each point in the simulation. For reference, the evolution of the total OA mass is shown in **(d)** as a function of the number of oxidation lifetimes (note the split y-axis and change in scale). Note the continuous evolution of the compound distributions.

ACPD
12, 3295–3356, 2012

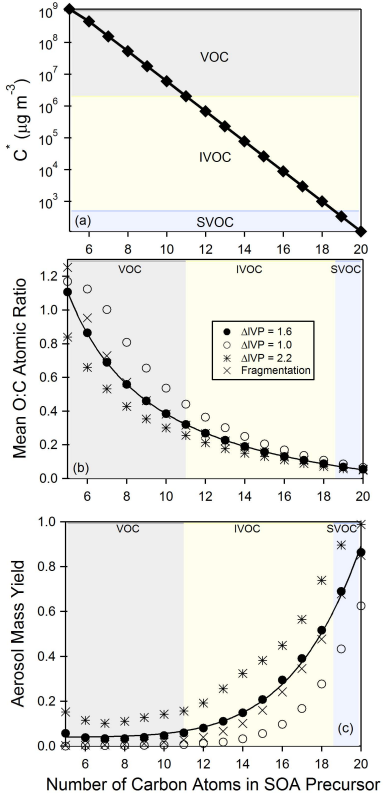

Fig. 2. **(a)** The relationship between volatility (C^*, in $\mu g\,m^{-3}$) and number of carbon atoms, showing the distinction between VOCs (gray), IVOCs (yellow) and SVOCs (blue). Also, the calculated mean O:C **(b)** and aerosol mass yield **(c)** are shown as a function of the number of carbon atoms in the SOA precursor. Results are shown for a variety of conditions with respect to fragmentation (see legend). The curves in **(b)** and **(c)** are power-law fits to the no-fragmentation case with $\Delta IVP = 1.6$. All calculations are for $C_{OA} = 10\,\mu g\,m^{-3}$ formed over 1 oxidation lifetime.

ACPD
12, 3295–3356, 2012

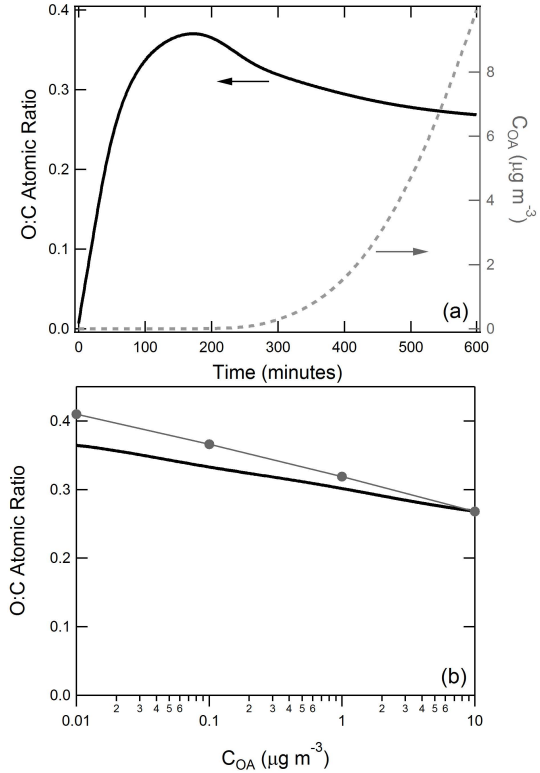

Fig. 3. **(a)** Temporal evolution of the mean aerosol O:C atomic ratio (left axis, black line) and the organic aerosol mass (C_{OA}, right axis, gray dashed line) over 1 oxidation lifetime. **(b)** The time-variation in the calculated O:C with C_{OA} shown over the instrumentally relevant range – i.e., >0.01 μg m^{-3}, corresponding to $t > 200$ min in **(a)**, black line. Shown for comparison is the O:C calculated after forming a specific amount of OA over 1 oxidation lifetime (gray circles). Calculations are for the no fragmentation case for $N_C = 12$ over 1 oxidation lifetime.

ACPD
12, 3295–3356, 2012

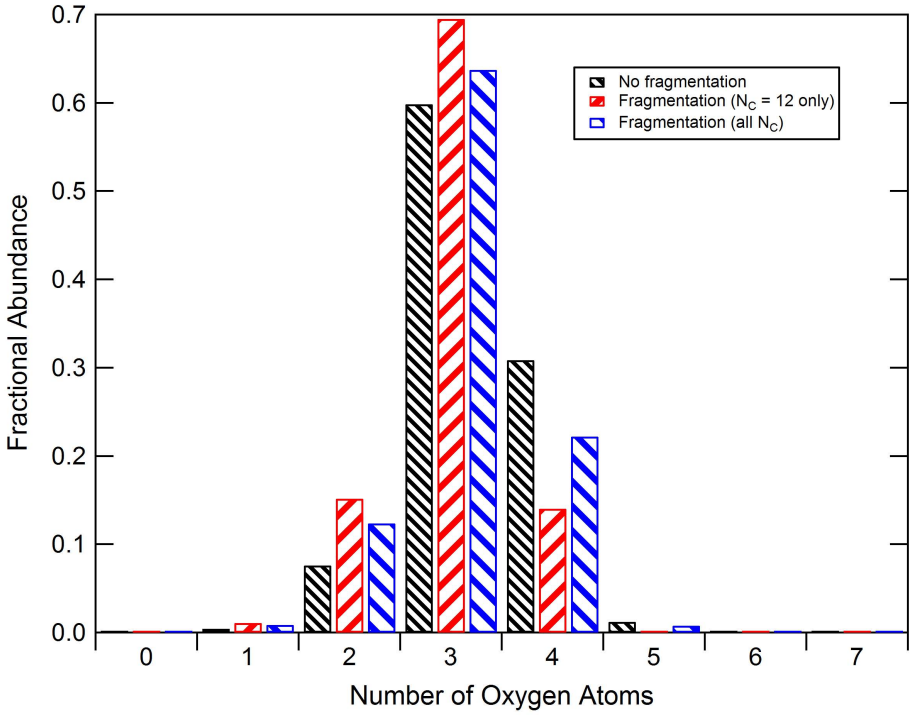

Fig. 4. Calculated distribution of oxygen atoms in the particle-phase after 1 lifetime of reaction for a $N_C = 12$ SOA precursor for cases without fragmentation and with fragmentation (see legend).

ACPD
12, 3295–3356, 2012

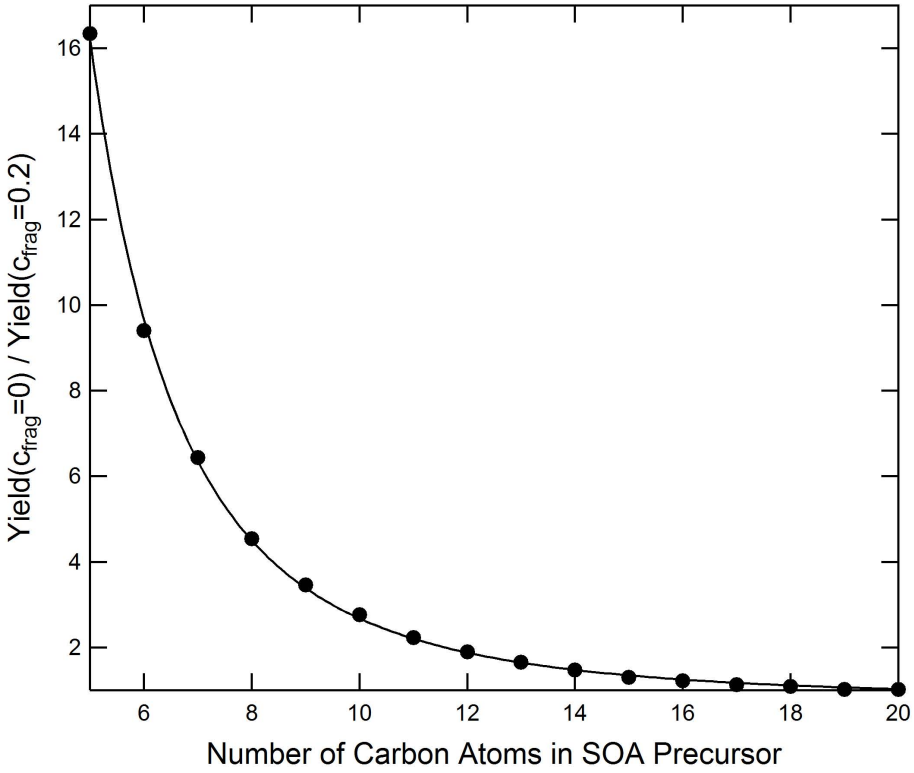

Fig. 5. The ratio between the aerosol yield calculated without and with fragmentation (assuming $c_{frag} = 0.2$, $\Delta IVP = 1.6$ and $C_{OA}(\tau_{OH} = 1) = 10\,\mu g\,m^{-3}$). The line is a power law fit.

ACPD
12, 3295–3356, 2012

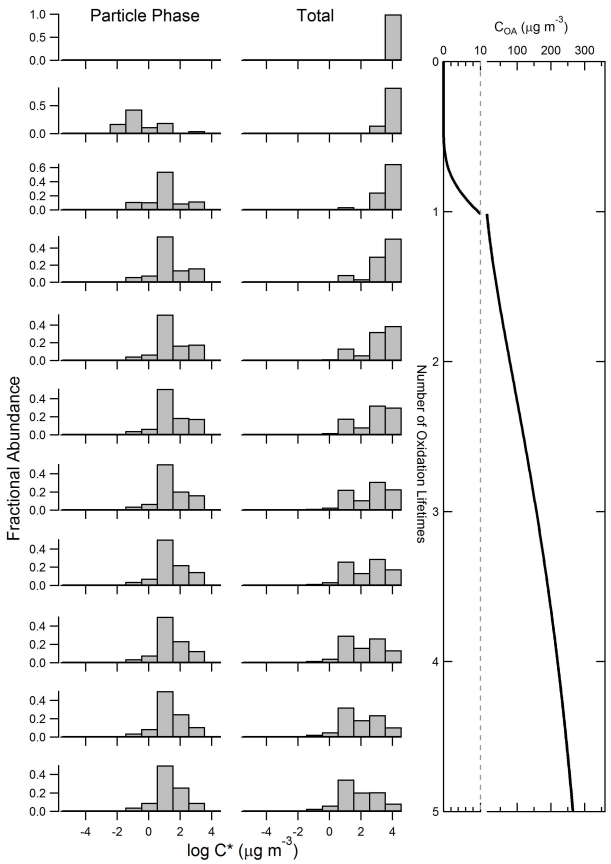

Fig. 6. Histograms showing the variation in the particle phase and total mass distributions when binned into logarithmically-spaced volatility bins as a function of the number of oxidation lifetimes. Calculations are for a N_C = 12 SOA precursor. For reference, the variation in the C_{OA} with lifetimes is shown.

ACPD
12, 3295–3356, 2012

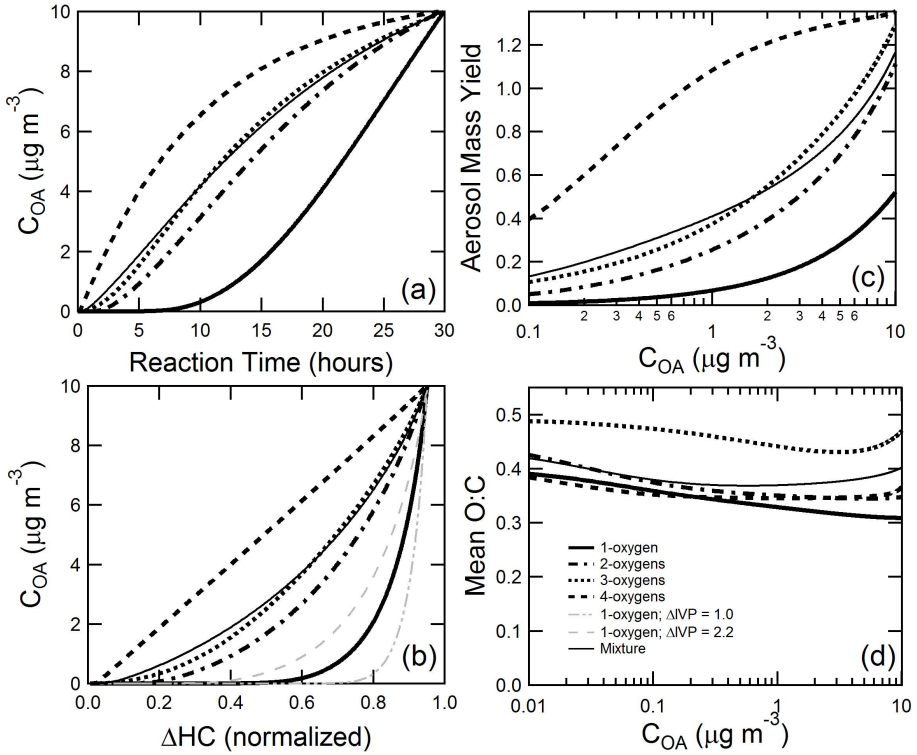

Fig. 7. The **(a)** temporal evolution of the aerosol mass, **(b)** variation of C_{OA} with the amount of SOA precursor reacted, **(c)** variation of aerosol yield with C_{OA}, and **(d)** variation of O:C with COA shown for the addition of 1, 2, 3 or 4 oxygen atoms per reaction for a $N_C = 12$ SOA precursor over 3 lifetimes of oxidation, assuming ΔIVP = 1.6. In panel **(b)**, growth curves are also shown for 1-oxygen per reaction with ΔIVP = 1.0 and ΔIVP = 2.2.

ACPD
12, 3295–3356, 2012

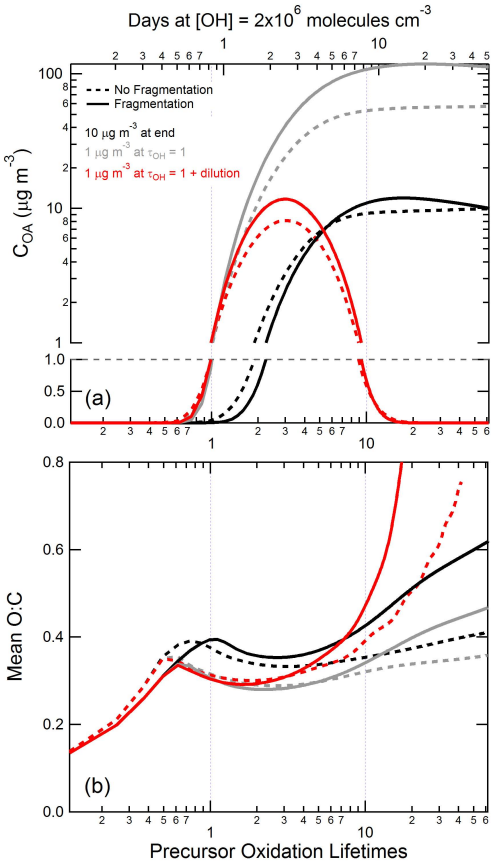

Fig. 8. **(a)** The variation in C_{OA} with the number of precursor oxidation lifetimes for a $N_C = 12$ precursor (see legend and text for specific conditions). The equivalent aging timescale is shown for reference (assuming 1 day = 12 h of daylight). Note the split axis and change from a log to linear scale for the y-axis. **(b)** The calculated mean O:C as a function of precursor lifetimes.

ACPD
12, 3295–3356, 2012

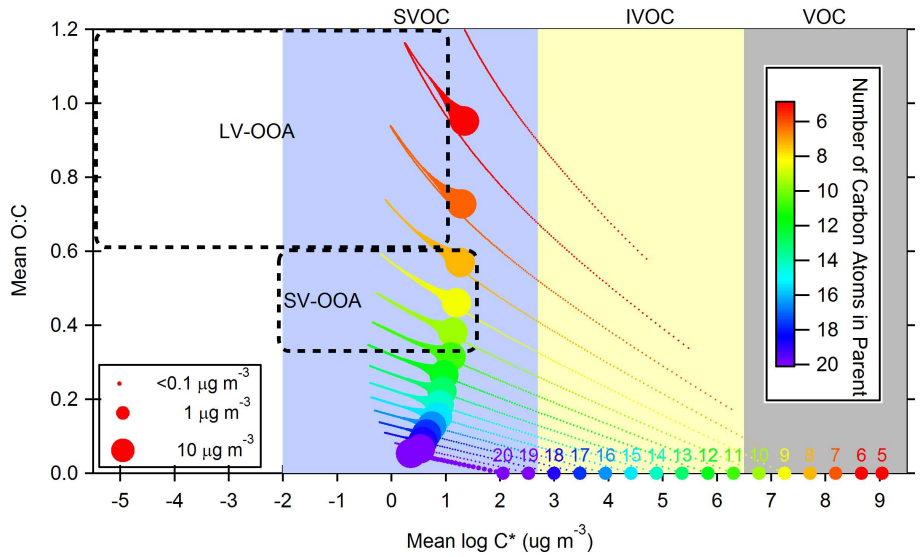

Fig. 9. The evolution of SOA formed from SOA precursor compounds with $5 \leq N_C \leq 20$ over 1 lifetime of reaction where $10\,\mu g\,m^{-3}$ SOA has been formed. Points are colored by the number of atoms comprising the SOA precursor and the symbol size corresponds to the amount of OA formed. Regions designating LV-OOA and SV-OOA are from Jimenez et al. (2009).

ACPD
12, 3295–3356, 2012

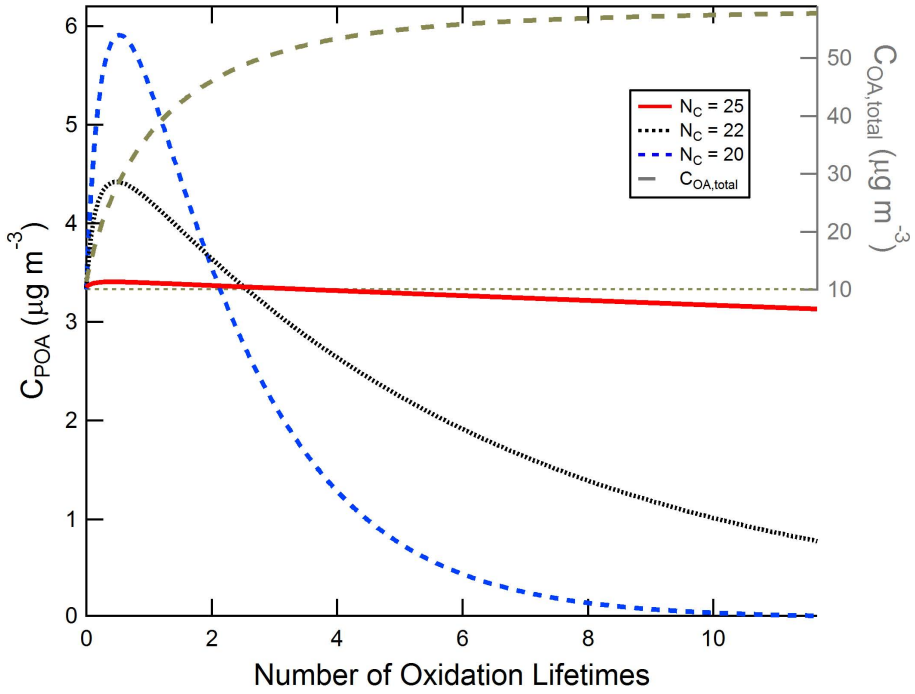

Fig. 10. Time-evolution of the abundance of "POA" species (i.e., SOA precursors initially present in the particle-phase) for a mixture of $N_C = 25$, 22 and 20 compounds (left axis). It is assumed that each compound contributes equally to the total initial particle mass ($C_{POA,total} = 10\,\mu g\,m^{-3}$). For reference, the change in the total OA mass is shown (right axis). This includes contributions of POA loss, oxidized POA formation and SOA formation.

ACPD
12, 3295–3356, 2012

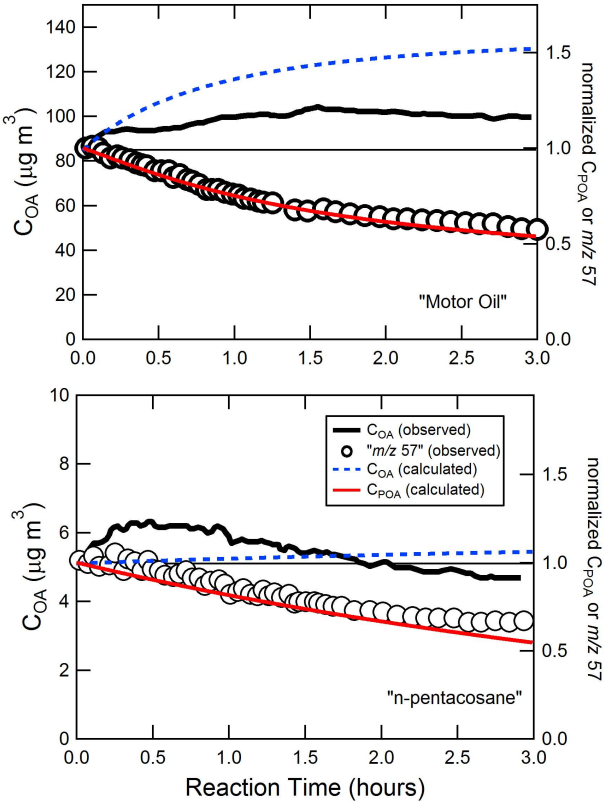

Fig. 11. The time-evolution of total OA mass (POA + SOA, including OPOA; left axis) or the normalized calculated total POA or observed POA tracer (*m/z* 57) (right axis) for photooxidation experiments of motor oil (top panel) or *n*-pentacosane (bottom panel). Observed values are taken from (Miracolo et al., 2010).

ACPD
12, 3295–3356, 2012

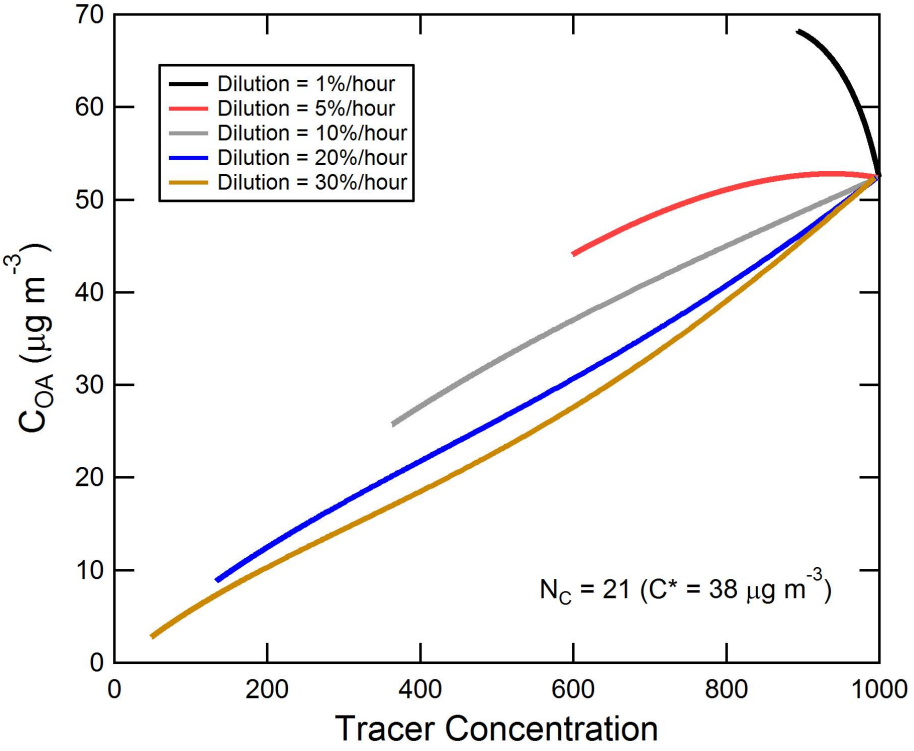

Fig. 12. Variation in the calculated C_{OA} with a conserved tracer concentration (initial = 1000) upon dilution + reaction at [OH] = 2×10^6 molecules cm^{-3} for different assumed dilution rates (see legend).

ACPD
12, 3295–3356, 2012

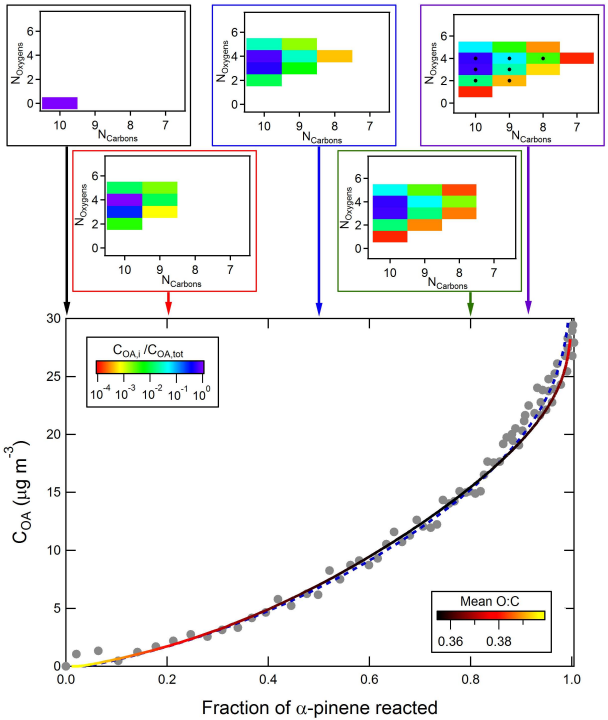

Fig. 13. Aerosol growth curve for α-pinene photooxidation under low-NO_x conditions comparing the calculated curve (line) to observations (points) (Ng et al., 2006). The calculated curve is colored by the mean O:C of the OA and was calculated using the fragmentation operator from Eq. (4); the blue dashed line uses P_{frag} from Eq. (5). The small graphs show the distribution of products, colored by mole fraction in the condensed phase, at various points throughout the reaction (indicated by arrows) in oxygen/carbon space. The points in the upper-right graph indicate structures for compounds that have been observed to exist in the condensed phase with measurable yields.

ACPD
12, 3295–3356, 2012

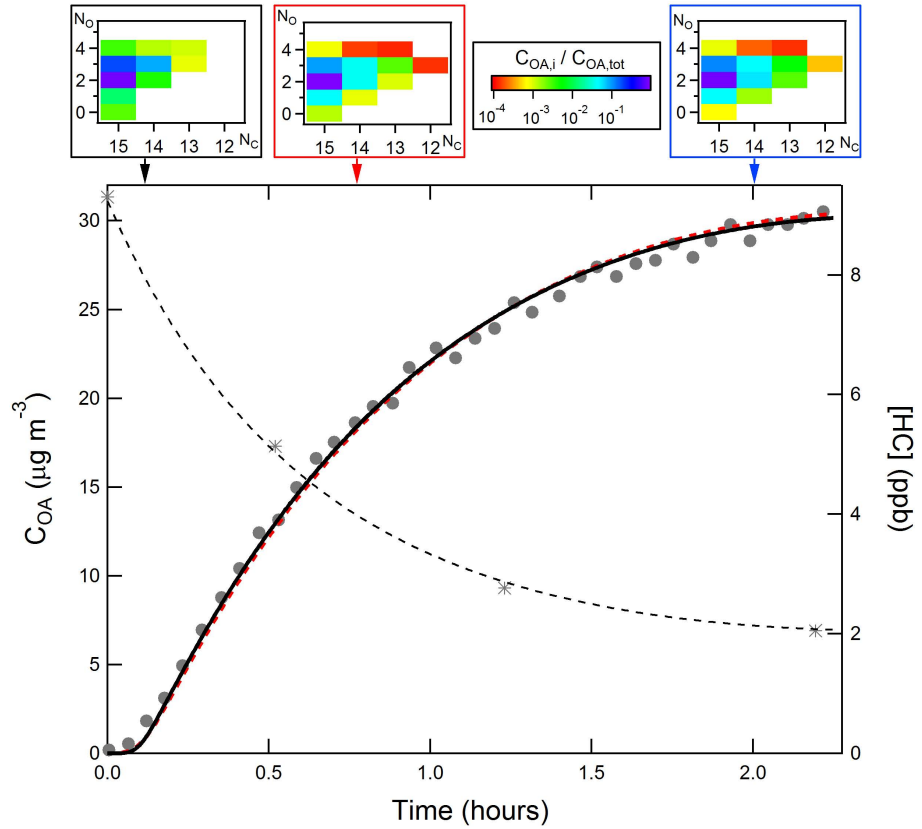

Fig. 14. The temporal evolution of C_{OA} (left axis) and [HC] (right axis) for photoxidation of pentadecane under high-NO_x conditions for the model (lines) and measurements (symbols: C_{OA} = • and [HC] = *). The solid black line uses the P_{frag} from Eq. (4) and the red line P_{frag} from Eq. (5). Measured values are from Presto et al. (2010). The insets show the distribution of products in the particle phase, colored by mole fraction, at various points throughout the reaction (indicated by arrows).

ACPD
12, 3295–3356, 2012